WATER RESOURCES RESEARCH, VOL. 36, NO. 12, PAGES 3499–3520, DECEMBER 2000

Conceptual model of the geometry and physics of water flow in a fractured basalt vadose zone

Boris Faybishenko,[1] Christine Doughty,[1] Michael Steiger,[1,2] Jane C. S. Long,[1,3] Thomas R. Wood,[4] Janet S. Jacobsen,[1,5] Jason Lore,[6,7] and Peter T. Zawislanski[1]

Abstract. A conceptual model of the geometry and physics of water flow in a fractured basalt vadose zone was developed based on the results of lithological studies and a series of ponded infiltration tests conducted at the Box Canyon site near the Idaho National Engineering and Environmental Laboratory. The infiltration tests included one 2-week test in 1996, three 2-day tests in 1997, and one 4-day test in 1997. For the various tests, initial infiltration rates ranged from 4.1 cm/d (4.75×10^{-7} m/s) to 17.7 cm/d (2.05×10^{-7} m/s) and then decreased with time, presumably because of mechanical or microbiological clogging of fractures and vesicular basalt in the near-surface zone, as well as the effect of entrapped air. The subsurface moisture redistribution was monitored with tensiometers, neutron logging, time domain reflectrometry, and ground-penetrating radar. A conservative tracer, potassium bromide, was added to the pond water at a concentration of 3 g/L to monitor water flow with electrical resistivity probes and water sampling. Analysis of the data shows evidence of preferential flow rather than the propagation of a uniform wetting front. We propose a conceptual model describing the saturation-desaturation behavior of the basalt, in which rapid preferential flow occurs through the largest vertical fractures, followed by a gradual wetting of other fractures and the basalt matrix. Fractures that are saturated early in the tests may become desaturated thereafter, which we attribute to the redistribution of water between fractures and matrix. Lateral movement of water takes place within horizontal fracture and rubble zones, enabling development of perched water bodies.

1. Introduction

Fluid flow and chemical transport in unsaturated fractured rocks are currently being studied with respect to the siting of radioactive waste repositories (e.g., Yucca Mountain, Nevada) and remediation of contaminated sites (e.g., Idaho National Engineering and Environmental Laboratory (INEEL), Idaho). The Department of Energy faces the remediation of several contaminated sites with fractured basalt vadose zones, where chemical and radioactive wastes released from shallow ponds and deep wells have traveled downward sporadically through narrow fracture pathways that are difficult, if not impossible, to detect. In addition, lateral spreading of water has occurred through systems of perched water zones that are poorly understood. Thus the behavior of contaminants at these sites has been very difficult to predict. Development of effective remediation procedures for these contaminated sites requires an appropriate conceptual model that describes the geometry of the flow domain and the physics of water flow through it. In general, conceptual models that describe water flow include a description of the hydrologic components of the system and how mass is transferred between these components. The development of a conceptual model is based on the analysis and simplification of data collected during field and laboratory experiments (Figure 1). A key difficulty with the procedure outlined in Figure 1 is that without a conceptual model we do not know what tests to conduct, what parameters to measure, where to place probes, or what probes to use. Consequently, the development of a conceptual model requires an iterative approach, in which we conduct a series of tests to obtain data and, concurrently, develop a conceptual model of water flow to refine our tests.

The unique feature of fractured rocks is that flow and transport processes are affected by the contrast in hydraulic conductivities of the fractures and porous matrix, which may be extreme and localized. For example, in fractured basalt, fractures with hydraulic conductivity as high as 30 m/d (3.5×10^{-4} m/s) [*Wood and Norrell*, 1996], or even higher [*Heath*, 1984], are imbedded in a rock matrix with hydraulic conductivity as low as 10^{-8} m/d (1.2×10^{-13} m/s). Water flow in a fracture network embedded in a low-permeability matrix depends strongly on the interconnection or connectivity of the fractures [*National Research Council Committee on Fracture Characterization and Fluid Flow*, 1996]. Often many, or in some cases nearly all, observable fractures play no significant role in flow, even when they appear to be interconnected [*Knutson et al.*, 1993; *Priest*, 1993]. Fractures may be nonconductive because apertures are closed under the ambient stress state or by mineral precipitation. Fracture conductivity may decrease during

[1]Earth Sciences Division, E. O. Lawrence Berkeley National Laboratory, University of California, Berkeley.
[2]Now at Erler and Kalinowski, Inc., San Mateo, California.
[3]Mackay School of Mines, University of Nevada, Reno.
[4]Idaho National Engineering and Environmental Laboratory, Idaho Falls.
[5]Now at Lawrence Livermore National Laboratory, Livermore, California.
[6]Department of Geological and Environmental Sciences, Stanford University, Stanford, California.
[7]Now at BP Amoco Exploration, Houston, Texas.

Copyright 2000 by the American Geophysical Union.

Paper number 2000WR900144.
0043-1397/00/2000WR900144$09.00

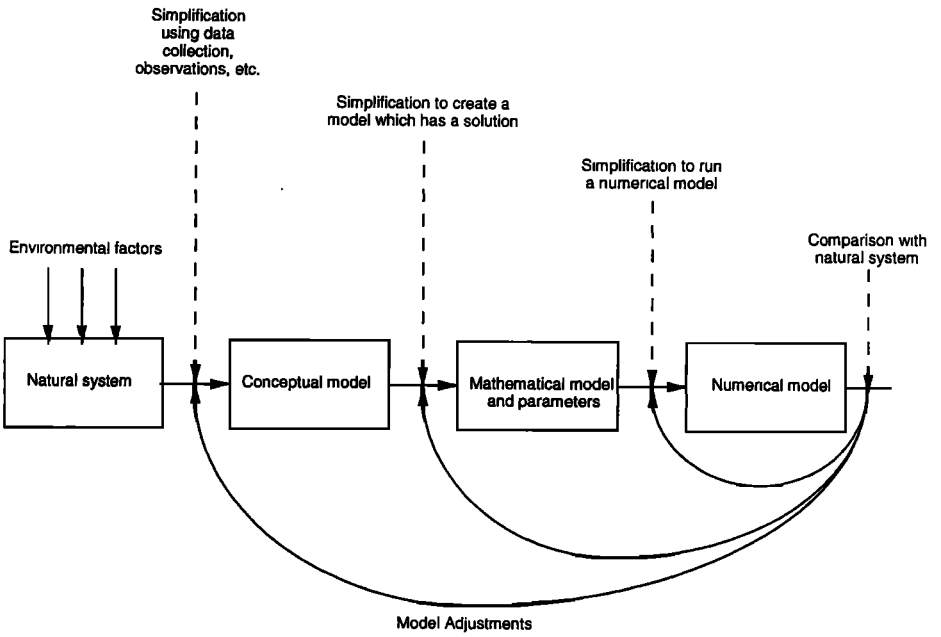

Figure 1. The relationship between different stages of an investigation showing how a conceptual model relates to field and numerical investigations.

an infiltration event owing to clogging, sealing, or air entrapment. The effects of capillary, viscous, and gravitational forces are relatively well understood for unsaturated porous media, but their coupling effects in fractured media are not well understood and cause uncertainty in predictions of flow and transport.

Over the past 20–30 years a number of authors have conducted field, laboratory, and modeling research on the development of conceptual models for flow and transport in unsaturated fractured rocks [e.g., *Evans and Nicholson*, 1987; *Peters and Klavetter*, 1988; *Wang and Narasimhan*, 1993; *Pruess*, 1999; *Pruess et al.*, 1999]. A series of water flow and solute migration experiments were conducted in unsaturated fractured chalk in the Negev Desert of Israel by *Nativ et al.* [1995], *Dahan et al.* [1998], and *Weisbrod et al.* [1998]. They designed a compartmental liquid sampler, which was inserted into a horizontal borehole, to collect infiltrating solution at multiple locations. They estimated the amount of water flowing through the fractures and imbibing into the matrix across the fracture walls and determined that under variable moisture content conditions the fracture aperture, roughness, and flow channels varied with time. They also noted that under field conditions the effective fracture aperture was more than 1 order of magnitude smaller than that expected based on laboratory conditions. *Or and Ghezzehei* [2000] studied water dripping into subterranean cavities in a fractured porous medium in order to improve estimates of dripping rates onto waste disposal canisters placed in caverns. These results suggest that conventional approaches and concepts, such as Darcy flow through a constant fracture aperture, may not be valid for characterizing unsaturated fractured rocks.

Several laboratory-scale investigations were conducted using natural fracture cores and fracture replicas to investigate factors and processes affecting flow and transport under controlled conditions at the centimeter to decimeter scale. For example, *Persoff and Pruess* [1995] injected a water-air mixture into a fracture replica under different flow rates and observed temporal instabilities of water and air pressure at the entrance and exit of the fracture as well as instabilities in the capillary pressure in the fracture. From their observations they concluded that the redistribution of entrapped air created spatial and temporal flow instabilities. *Glass et al.* [1991], *Lenormand and Zarcone* [1989], *Nicholl et al.* [1993, 1994], and *Su et al.* [1999] observed phenomena of preferential flow and channeling in fractures or fracture replicas.

Despite the value of laboratory studies to elucidate fundamental aspects of fracture flow, there remains a lack of understanding of how real systems composed of multiple fractures and other hydrogeological components behave at the field scale, which forces researchers to make many assumptions, most or which are site-specific, and to oversimplify models [*Eaton et al.*, 1996]. To improve the models, we need to investigate under what conditions fractures conduct water, the effects of fracture infilling materials and asperity contacts, when unsaturated fractures constrain flow by playing the role of capillary barriers, and how fracture-matrix interactions affect flow.

Field measurements in unsaturated fractured rocks of the vadose zone have proven challenging because of difficulties with drilling and completion of boreholes, setting up instrumentation to provide access to fractures, and collecting water from fractures and matrix for chemical analysis. The design of borehole tests and the interpretation of data in fractured rocks are complicated because the response in a monitoring well may only be from a single fracture [*National Research Council Committee on Fracture Characterization and Fluid Flow*, 1996]. In this case, measuring the test response is equivalent to measuring the response in a single pore in a porous medium. Therefore "point" measurements in a fractured system cannot reveal processes that result from the interaction of features at many different scales that are related to each other in a complex manner.

The purpose of this paper is to discuss the development of a conceptual model of the geometry of the flow domain and the

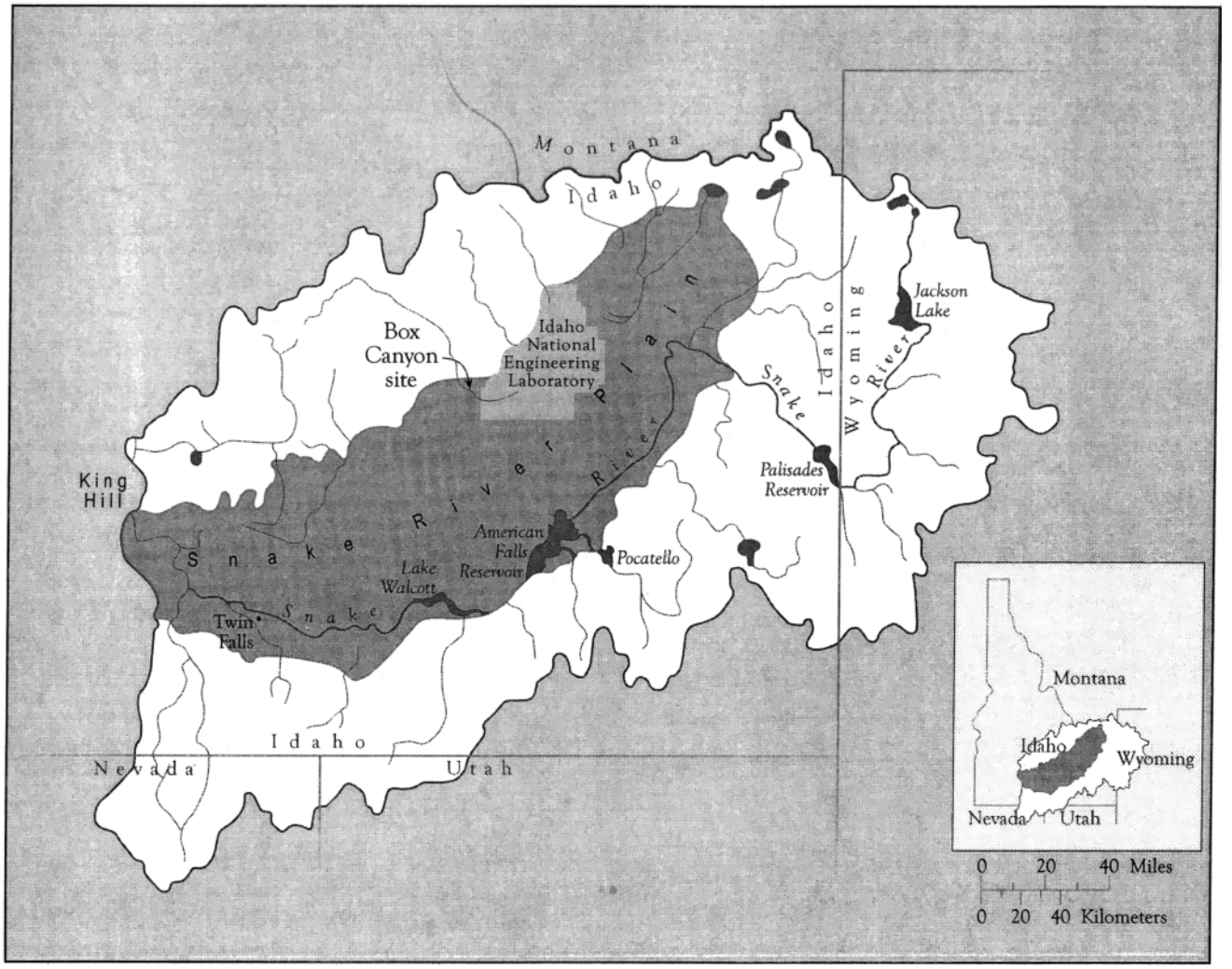

Figure 2. Map of the Eastern Snake River Plain and the location of the Box Canyon experimental site.

physics of water flow in a fractured basalt vadose zone based on results from a detailed site characterization and a series of ponded infiltration tests using a tracer. The field experiments were conducted at the Box Canyon site, located in the Eastern Snake River Plain near INEEL (Figure 2). The area called Box Canyon is adjacent to the Big Lost River. The Box Canyon site is an environmentally clean analog site for contaminated sites at INEEL. Minimal soil cover and a nearby cliff face exposure provide an excellent opportunity to study the relationships between the fracture pattern and the hydrogeologic response to the infiltration tests.

In this paper, after an overview of the Snake River Plain geology, we present a preliminary conceptual model for water flow in a fractured basalt vadose zone, based on the analysis of data obtained during the Large Scale Infiltration Test (LSIT) conducted at INEEL. The lithology and fracture pattern at the Box Canyon site, the results of a series of ponded infiltration tests, and an augmented conceptual model of the geometry and physics of flow are then presented.

2. Snake River Plain Geology

The Snake River Plain is primarily composed of fractured Quaternary basalt flow units, interlayered with sedimentary deposits [*Welhan and Reed*, 1997]. Sedimentary interbeds may separate basalt flow units that were formed at widely separated times, and their thickness may range from a few centimeters to as much as 15 m. Some have great areal extent, while others are of limited extent. Basalt flow units are composed of a number of basalt flows arising from the same eruption event. Individual basalt flows generally consist of multiple lobes that are elongated in one direction, giving them a finger-like or lenticular structure. Typical lobe dimensions are 3–12 m thick and 20–60 m wide, with lengths of up to a kilometer [*Sorenson et al.*, 1996]. Basalt flows are typically highly fractured or rubblized at the flow margins. Geophysical logging and borehole coring results suggest that the total basalt thickness in the Snake River Plain may exceed 3 km. A more detailed description of the lithology of the Snake River Plain is given by *Knutson et al.* [1993].

3. Preliminary Conceptual Model Based on Results of the Large-Scale Infiltration Test

The LSIT was conducted at the Radioactive Waste Management Complex of INEEL in 1994 to characterize water flow on the scale of several hundred meters (the macroscale) [*Wood and Norrell*, 1996]. A 26,000 m^2 infiltration basin was flooded

with water for a period of 36 days, and several tracers were added to the basin water 6 days after the onset of flooding [*Newman and Dunnivant*, 1995]. The existing conceptual model for flow at the macroscale assumed that the Snake River Plain basalt behaved as an oversized porous medium, in which the network of rubble zones surrounding individual basalt flows represented the pore space and the basalt flows represented the mineral grains. It was assumed that the permeability of the intra-basalt-flow fractures was negligible in comparison with that of the inter-basalt-flow rubble zones. Consequently, the large aspect ratio of the individual basalt flows (lateral extent significantly exceeds thickness) would impart a large anisotropy to the effective permeability of the medium (horizontal permeability significantly exceeds vertical permeability). Because of the macroscale anisotropy, extensive lateral spreading was expected to accompany infiltration, so a large fraction of the monitoring wells were located outside the footprint of the infiltration pond. Of the 101 monitoring locations, water was recovered from 30, and the tracer, Se-75, assumed to be conservative, was found in only 26. No monitoring locations outside the footprint of the infiltration pond showed water or tracer arrival in the vadose zone, except in perched water zones just above a sedimentary interbed located at a depth of ~70 m. The shapes of the breakthrough curves varied significantly between the different locations. *Newman and Dunnivant* [1995] were able to model 10 of the 26 tracer breakthrough curves using a one-dimensional model of advective-diffusive transport through a homogeneous porous medium with a constant water velocity. The low success rate of the one-dimensional model indicated that a volume-averaged macroscale conceptual model was inappropriate for interpreting field-scale measurements within a fractured basalt vadose zone.

In order to improve the conceptual model and to interpret the spatial and temporal distribution of tracer in the subsurface, a schematic fracture pattern keyed to representative breakthrough curves (BTC) from the LSIT was developed (Figure 3). The analysis of a variety of the BTC shapes implies that the detection of tracer depends on the location of the sampling point within the fracture system and the connectivity of the fractures supplying water to that point. The BTCs do not produce a unique correlation between the distance from the tracer source and tracer arrival time. For example, although tracer-free water infiltrated the basin for 6 days prior to the addition of tracers, the first water observed in several wells contained tracer (locations 2, 5, and 6 in Figure 3). In addition, tracer-free water was observed in several lysimeters throughout the course of the test (locations 3 and 4).

Despite the presence of the inter-basalt-flow rubble zones in the vadose zone at the LSIT site, lateral spreading was only significant over the sedimentary interbed. It appeared that intra-basalt-flow vertical fractures contributed considerably more to the overall vertical permeability than had previously been assumed. To better understand this contribution, we focused our studies at the Box Canyon site on the intermediate scale (several meters) over the central portion of a single basalt flow. At this scale the internal fracture pattern within the basalt flow is assumed to be a major factor affecting water flow.

4. Lithology and Fracture Pattern at Box Canyon

The surface of the Box Canyon site consists of exposed weathered basalt and soils (clays and silts), which infill the near-surface fractures and basalt column joints. The depth to the regional aquifer is ~200 m, and a perched water zone is located at a depth of ~20 m. Along the vertical Box Canyon cliff face, located ~30 m from the infiltration pond, two distinct basalt flows separated by a rubble zone can be seen.

The connectivity of the fracture pattern and its relationship to other geological features are of critical importance. A fracture map provides the best illustration of the fracture spatial distribution, persistence, and the size and shape of fracture-bounded blocks [*Laubach*, 1991]. The two-dimensional map (a vertical cross section) of the fracture pattern in the uppermost basalt flow exposed on the side of the cliff at Box Canyon is shown in Plate 1. The basalt flow is divided into upper and lower zones of distinctly different fracturing because of different cooling rates and temperature gradients in the upper and lower portions of the basalt flow. Plate 1 also depicts fractures of varying length propagating from the top of the basalt flow that connect the surface with major vertical and horizontal fractures, whereas the fractures propagating upward from the bottom of the basalt flow are less well connected and may be considered dead-end, or nonconductive, fractures.

Site characterization, including cliff face mapping, borehole logging, and cross-hole gas-phase interference tests, revealed that the fractured basalt vadose zone is composed of the following geological components (shown in Plate 1): (1) soils and flow top breccia and boulders, (2) near-surface soil-infilled fractures, (3) upper and lower vesicular zones, (4) isolated vesicular layers, (5) massive basalt, (6) a central horizontal fracture zone, and (7) a flow contact rubble zone.

The discontinuities that affect water flow the most in fractured basalt are column-bounding fractures (also called joints [*Engelder*, 1987; *Priest*, 1993]), intrabasalt fractures, fracture zones, and rubble zones. Column-bounding fractures in basalt usually form a polygonal network, created perpendicular to the cooling isotherm due to thermal contraction of basalt lava. Using fracture maps of seven basalt flows below and adjacent to the Box Canyon site, we determined the horizontally averaged spacing between fractures as a function of depth (Figure 4). The spacing between fractures for several basalt flows, likely of the same eruption, is markedly similar and exhibits an increase in spacing with depth in the upper two thirds of the flow thickness. The base of each basalt flow shows an inverted pattern, in which the lower part of the flow contains a smaller spacing between fractures than the center of the flow. At the exposed upper surface of the basalt flow the spacing between fractures is as low as 0.3 m. However, it is clear that some material has been removed from the upper exposures by weathering, thus removing the basalt with the smallest fracture spacing that is often present in the uppermost 2–3 cm of material in an unweathered basalt flow. Overall, the upper two thirds of the basalt flow is characterized by small fracture spacing and thus has more fractures than the lower third. In some basalt flows, there is a region near the center of the basalt flow that contains highly fractured rock that does not display the columnar style of fracturing [*Long and Wood*, 1986; *Tomkeieff*, 1940]. These subhorizontal central fracture zones are present in ~40% of basalt flows examined at Box Canyon, and one is observed below the infiltration site (Plate 1). On the basis of the results of experiments on core samples by *Knutson et al.* [1990] the porosity of the basalt matrix ranges from 20 to 40% with an arithmetic mean porosity of 19.2%, and the geometric mean permeability is 2.24×10^{-15} m^2 (the mean is biased toward low permeability because permeabilities greater

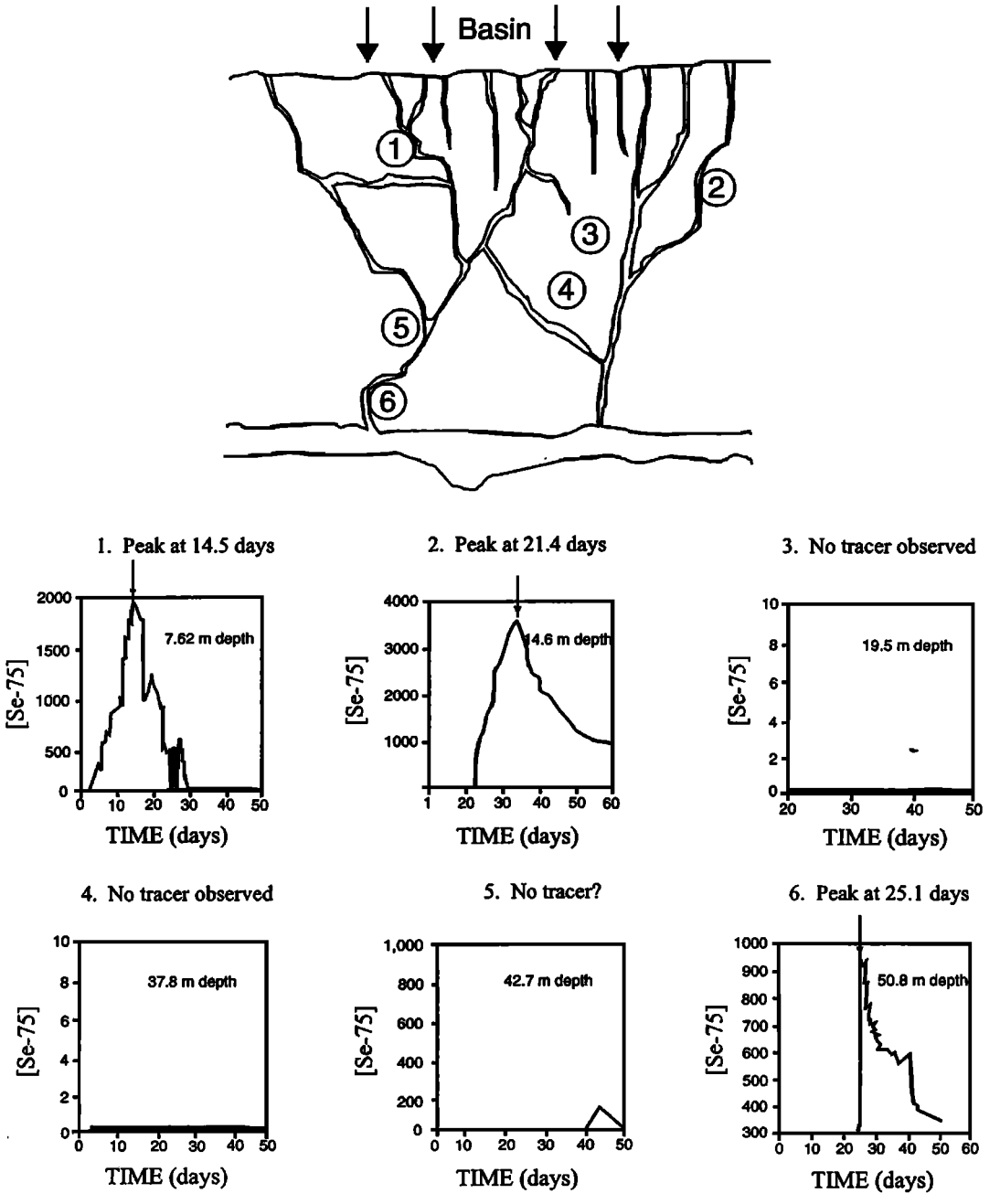

Figure 3. A conceptual model of a fracture pattern (not to scale) and (a) the types of flow paths and (b) different tracer breakthrough curves determined during the LSIT. The numbers on Figure 3a indicate the locations of lysimeters for which breakthrough curves are shown: (1) multimodal BTC due to a confluence of flow from multiple conductive fractures, (2) single-peak BTC in a single conductive fracture, (3) very slow diffusion of the tracer in a saturated dead-end fracture, (4) no tracer arrival in a low permeability massive basalt, (5) diffusion of the tracer in vesicular basalt near a conductive fracture, and (6) delayed and abrupt tracer arrival in a deep horizontal fracture or rubble zone. On Figure 3b, the horizontal axis is the time since the tracer was introduced in the pond, and the vertical axis is activity of Se-75 in pCi/L. BTC curves are from *Newman and Dunnivant* [1995].

than 10^{-12} m^2 from vesicular zones were not included in this calculation).

The fracture distribution observed at the Box Canyon cliff face was simplified and idealized in order to construct the simple four-generation "tree" model shown in Figure 5. The model shows that the largest basalt column is subdivided into several columns toward the top of the flow. This model also shows the branching (bifurcation) phenomenon for individual fractures, which may cause preferential flow paths and multiple flow paths leading to a given point. The model shown in Figure 5 indicates that in order to represent all geological components of a basalt flow the minimal domain for a geological investigation should extend from the top to the bottom of the basalt flow and its width should coincide with the maximum spacing

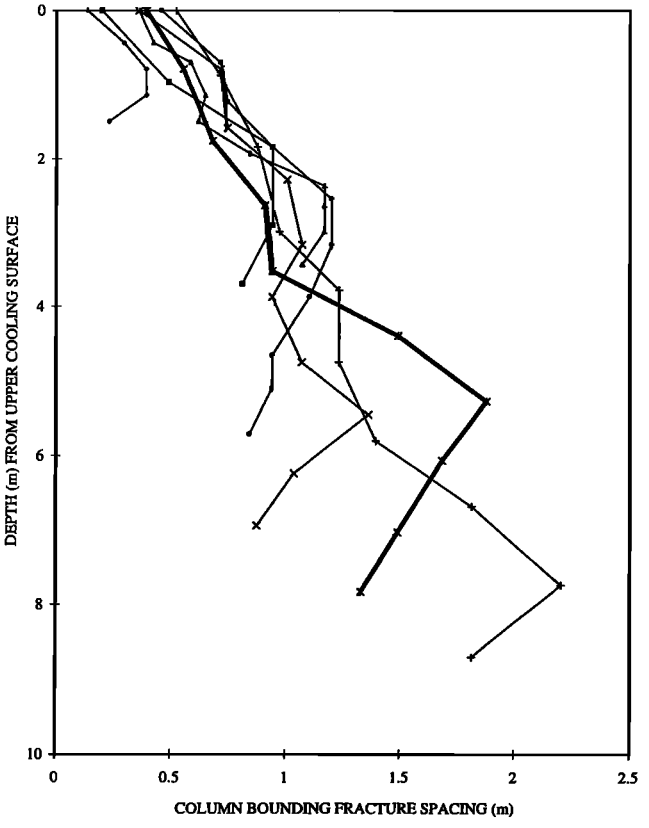

Figure 4. Column-bounding fracture spacing as a function of depth for seven basalt flows under (thick line) and adjacent to the Box Canyon infiltration pond.

between the columnar joints. At the Box Canyon site the average spacing between columnar joints is 0.46 m at the surface, 2.0 m near the center of the basalt flow, and 1.3 m at the bottom. The maximum spacing near the center of the flow is from 3.5 to 4 m.

5. Methods and Results of the Box Canyon Infiltration Tests

5.1. Design of Instrumentation Used at the Box Canyon Site

5.1.1. Site layout and instrumentation. Over the course of 3 years (1995–1997), 38 vertical and inclined boreholes were drilled (diameters of 10–15 cm) and logged (natural gamma and caliper measurements, downhole video recording, borehole scanning, and core description) to provide information about the types of fractures, the depth of soil infilling the fractures, the occurrence of vesicular zones, and the locations of fracture zones and rubble zones [*Faybishenko et al.*, 1998a, 1998b]. Plate 2a shows a three-dimensional view of the borehole layout. In 1995, three groups of 20 wells were drilled to study the geology of the site and to conduct hot air injection [*Long et al.*, 1995] and ambient air injection tests [*Benito et al.*, 1999], including vertical wells of series I (depths of 12 m) that intersected the first rubble zone, vertical wells of series II (depths of 18.3–22.5 m) that intersected several rubble zones, and inclined wells (30° from vertical) of series S (lengths of 4.9–21.2 m) that intersected one or several rubble zones. An example of the geological information obtained from series I and II wells is shown in Plate 2b.

In 1996, three groups of 16 wells were drilled to install monitoring instrumentation, including vertical wells of series T (depths of 3–6.7 m), and inclined wells (27°–45° from vertical) of series E and R (lengths of 18.3–22.9 m). In 1997, after interpretation of the results of the 1996 infiltration test, which showed a zone of preferential flow between wells R1 and R2, two additional inclined wells (R5 and R6) were drilled between existing R wells. Note that inclined boreholes were mostly drilled from the outside of the pond to reduce the disturbance to the pond surface and to intersect more vertical column-bounding fractures to better characterize the three-dimensional geometry of flow below the pond.

The types of instrumentation used during the infiltration tests are summarized in Table 1. A more detailed description of the instrumentation is given by *Faybishenko et al.* [1998b]. All the instruments were installed in boreholes using the following method of borehole completion [*Faybishenko et al.*, 1998d]. The instruments were attached to the outer faces of polyethylene packers mounted onto sections of 3.5-cm OD PVC manchette pipe, and the sections were glued together to form a continuous string of instruments placed at preselected depths. After the string with the probes was lowered into a borehole, the packers and the space between the packers were infilled with impermeable polyurethane resin, thus pressing the instruments against the borehole walls. This completion method ensured that no water flow occurred through the borehole.

On the basis of the geometric conceptual model of the fracture pattern we determined that the scale of the infiltration tests should be of the order of 8 m, so that hydrological processes are characterized on a scale that includes at least one or two major column-bounding fractures (their maximum spacing is 4 m at the center of the flow). Two designs of a 7 m by 8 m pond berm were used. In 1996, the berm was constructed using bags filled with crushed basalt and injected with polyurethane resin in order to create a watertight barrier. However, this design did not prevent water leakage at several locations beneath and through the berm during the first 1–2 days of the test. For the remainder of the test the water leakage through the berm to the area outside of the pond was <10% of the infiltration rate into the subsurface within the pond. In 1997, a

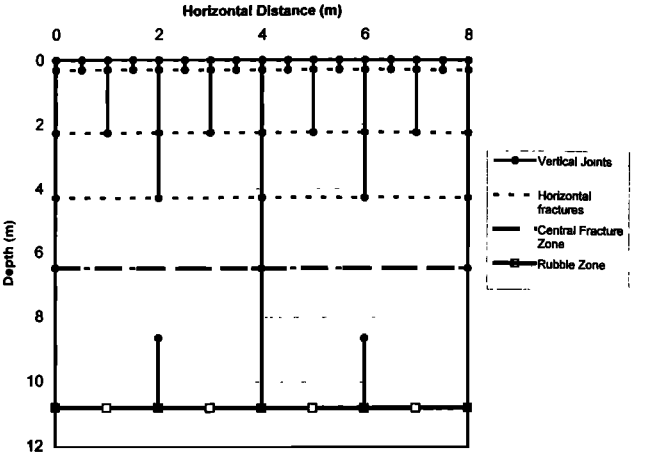

Figure 5. A conceptual tree-type model of the fracture pattern and fracture connectivity of the basalt flows. Note that nonconductive fractures originating from vertical fractures are not shown.

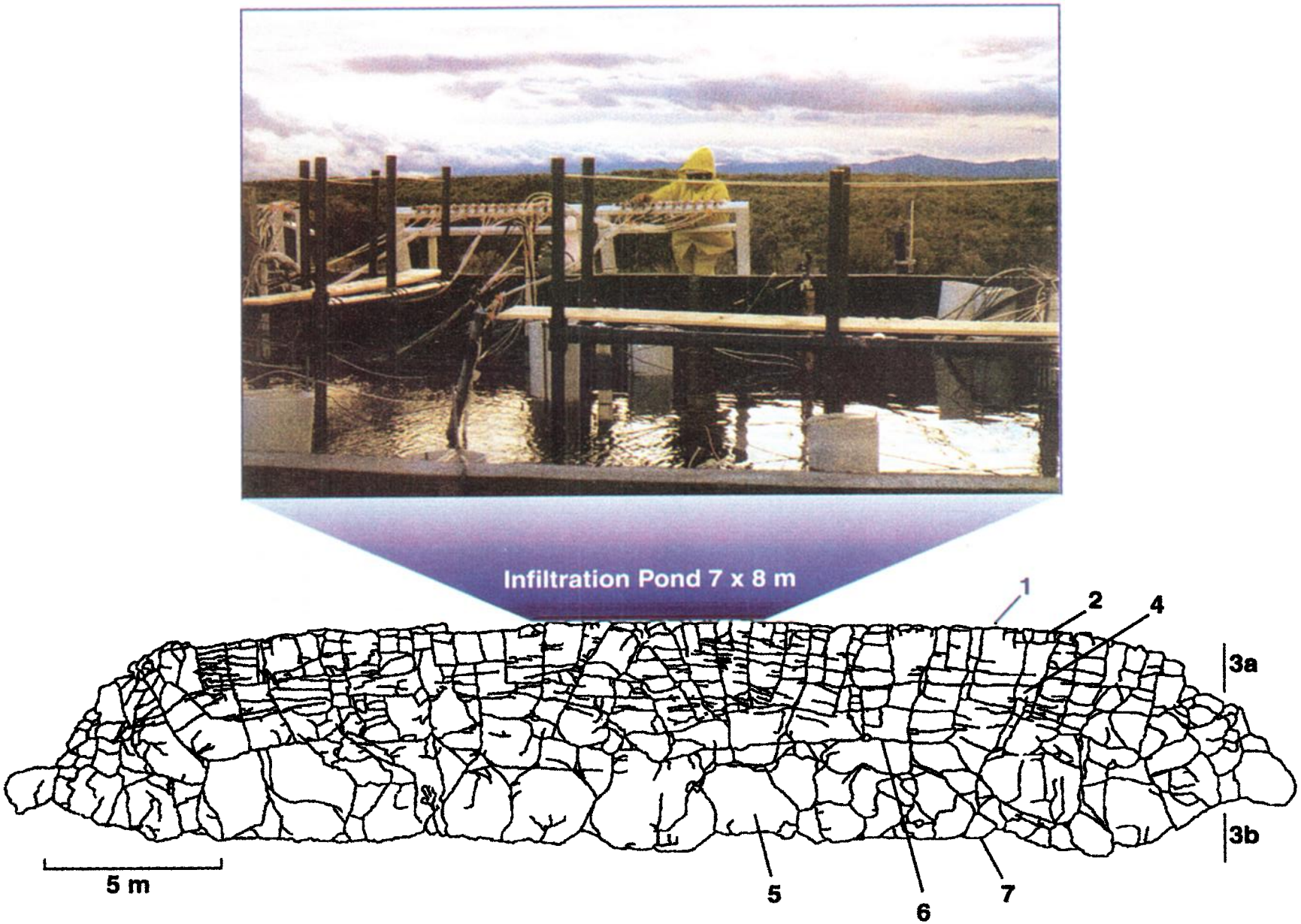

Plate 1. A photo of the Box Canyon infiltration pond and a two-dimensional map of the fracture pattern at the vertical basalt outcrop, showing the main functional geological components affecting water flow: (1) soils and flow top breccia and boulders, (2) near-surface soil-infilled fractures, (3) upper and lower vesicular zones, (4) isolated vesicular layers, (5) massive basalt, (6) central fracture zone, and (7) flow bottom rubble zone.

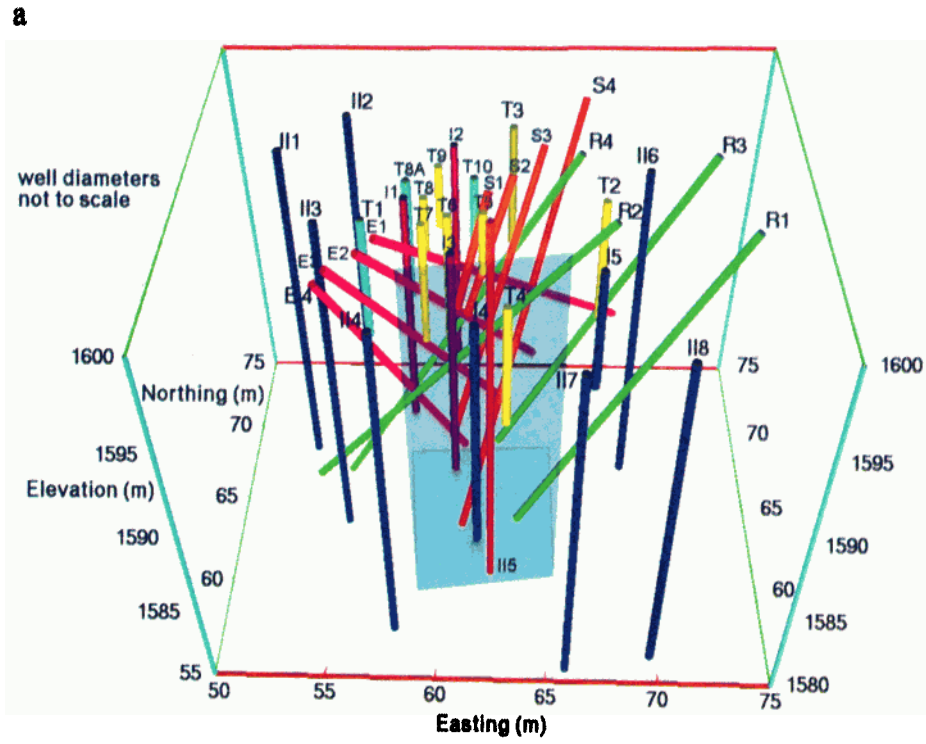

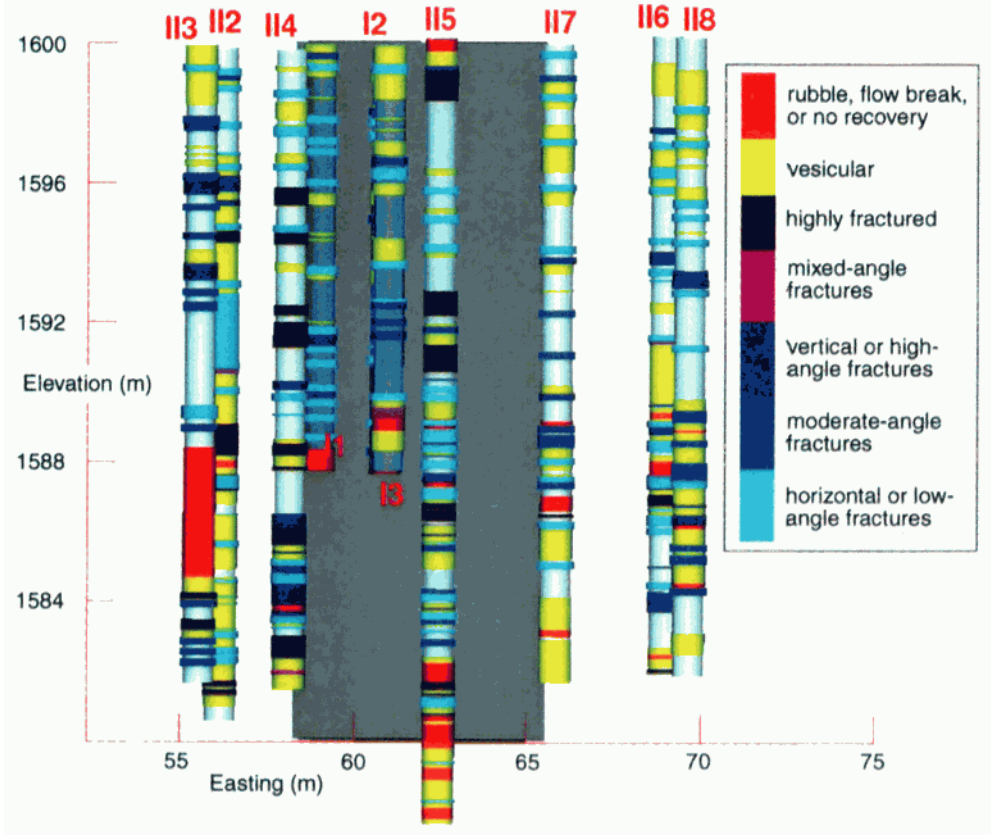

Plate 2. (a) Perspective view of well layout at the Box Canyon field site; purple, open, uncased wells outside the pond; gold, yellow, and magenta, backfilled, instrumented wells; green and teal, open, cased wells for ground-penetrating radar (GPR) and neutron logging. The footprint of the infiltration pond is shown shaded. A plan view of the Box Canyon site is given by *Doughty* [this issue, Figure 1a]. (b) Lithologies obtained from core (white background) or borehole televiewer (gray background) for selected vertical boreholes, with locations shown projected onto the easting axis of the site map shown in Plate 2a. The footprint of the infiltration pond is shown shaded. Note that vertical fractures may not be identified in vertical boreholes and are likely underrepresented.

Table 1. Summary of the Types of Data Collected and the Instrumentation Used During the Infiltration Tests at the Box Canyon Site

Type of Data	Type of Instrumentation	Source
Cumulative volume of water supplied into the pond	water flow totalizer	*Faybishenko et al.* [1998b]
Evaporation rate	evaporation pond	
Local infiltration rates at several locations within the pond	25-cm-diameter infiltrometers	*Faybishenko et al.* [1998b]
Water pressure	tensiometers with water-filled connecting tubes, pressure transducers at the surface	SoilMoisture, Inc., Santa Barbara, Calif.
Water and tracer samples	suction lysimeters: single chamber (0–20 feet, 0–6 m) double chamber (20–50 feet, 6–15 m)	SoilMoisture, Inc., Santa Barbara, Calif.
Changes in moisture regime	CPN 503DR hydroprobe	*Zawislanski and Faybishenko* [1999]
	Time domain reflectometry (TDR) using the Trase System	SoilMoisture, Inc., Santa Barbara, Calif.
	ground-penetrating radar (GPR)	*Hubbard et al.* [1997], *Peterson et al.* [1997], and *Vasco et al.* [1997]
Temperature	thermistors	*Faybishenko et al.* [1998b]
Electrical resistivity (ER)	miniature ER probes	*Lee et al.* [1998]
Water level in open boreholes	depth to water table meter	*Faybishenko et al.* [1998b]

small trench (15 cm high by 15 cm wide) was cut into the basalt at the location of the previous berm and a permanent concrete wall was constructed that practically eliminated water leakage beneath and through the berm.

5.1.2. Design of the infiltration tests. A series of ponded infiltration tests was designed to mimic episodic surface-flooding events that occur during large rainstorms or snowmelt events. This is the extreme condition for maximum infiltration and contaminant transport from the surface to the water table. From August 27, 1996, through September 9, 1996, a ponded infiltration test (test 96-1) was conducted by maintaining water at a spatially averaged depth of 23 cm above the uneven land surface. A tracer test was conducted midway through test 96-1 by adding a slug of a potassium bromide (KBr) solution to the pond water on September 2, 1996, yielding an average tracer concentration in the pond of approximately 3 g/L. The water supply to the pond was halted for 2 days so the tracer was not diluted; thereafter the water supply was reestablished to maintain a constant water level.

A series of four infiltration tests was conducted from September 11, 1997 through November 3, 1997 (tests 97-1 through 97-4). In each of these tests a fixed volume of water containing 3 g/L of KBr infiltrated for 2 days (during test 97-4, the solution infiltrated for 4 days), and then the remaining solution was pumped out to allow ambient air to enter the subsurface. The purpose of this design was to keep the concentration of the tracer constant in the pond during infiltration. These tests were also designed to decrease the effects of exhaustion processes such as in washing and swelling of colloids, which lead to a decrease in the infiltration rate with time, by providing intermittent periods of drying between each test. Periodic flooding is also thought to contribute to a chaotic component of flow in the subsurface, the subject of another investigation being conducted at the Box Canyon site [*Faybishenko et al.*, 1998c]. Table 2 summarizes the volume of water and mass of salt that infiltrated during each test.

5.2. Main Characteristics of Flow and Transport During the Infiltration Tests

5.2.1. Infiltration rate. To analyze the infiltration rate data obtained in the field, we first determined the cumulative volume of water that infiltrated into the subsurface by subtracting the cumulative volume evaporated from the cumulative volume supplied to the infiltration pond at each time interval. A Horton-type equation was used to fit the data of cumulative volume infiltrated [*Jury et al.*, 1991]

$$q = i_f t + (1/\beta)(i_0 - i_f)[1 - \exp(-\beta t)], \quad (1)$$

where q is cumulative water volume infiltrated per unit area (cm^3/cm^2), t is time (days, from the time when a constant water level was established), and the fitting parameters are i_0, initial infiltration rate (cm/d); i_f, final infiltration rate (cm/d); and β, exponential decay parameter.

Table 2. Summary of Volumes of Water and Masses of Tracer (KBr) Supplied to the Pond During the Infiltration Tests at the Box Canyon Site

	Start of Ponding		End of Ponding			
Test	Date	Time, LT	Date	Time, LT	Volume of Water Infiltrated, m^3	Mass of Salt Infiltrated, kg
96-1	Aug. 27, 1996	1227	Sept. 9, 1996	1100	25.00	38.64
97-1	Sept. 11, 1997	1215	Sept. 13, 1997	1245	5.42	16.26
97-2	Sept. 18, 1997	1456	Sept. 20, 1997	1646	5.01	15.03
97-3	Oct. 2, 1997	1540	Oct. 4, 1997	1600	3.91	11.73
97-4	Oct. 31, 1997	1351	Nov. 3, 1997	1500	6.79	20.37
97 totals					21.13	63.39

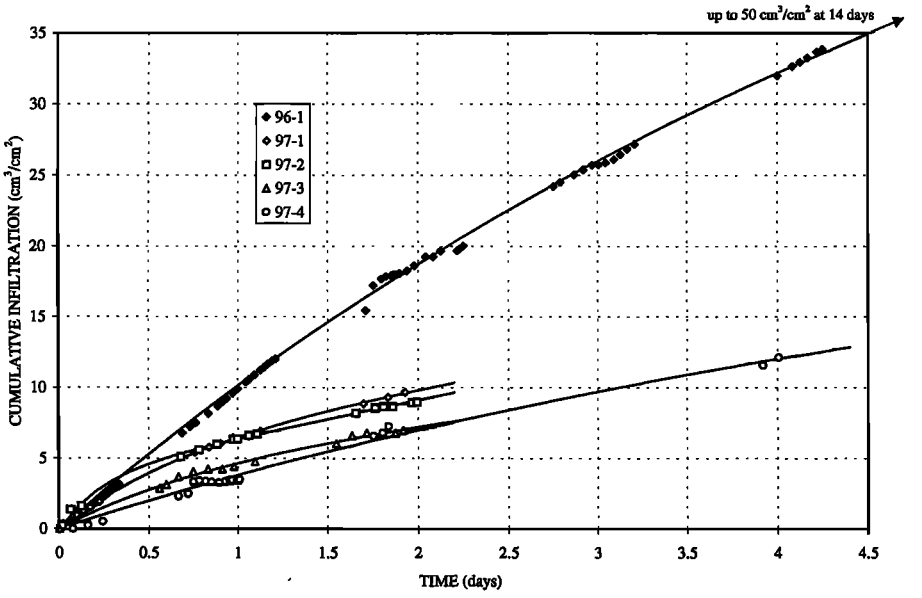

Figure 6. Time variation of the cumulative total volume of water infiltrated during the tests. The fitted lines are from a regression analysis using equation (1). Test 96-1 was conducted for 14 days; however, only 4.5 days are shown.

The experimental data and fitting curves are shown in Figure 6, and the fitting parameters for each test, which were determined using a least square nonlinear regression of Horton's exponential function, are summarized in Table 3. Note from Table 3 that in order to compare fitting parameters for all tests, we calculated these parameters for two cases: (1) assuming that the tests lasted only 2 days and (2) for the entire duration of tests given in Table 2 because tests 96-1 and 97-4 lasted longer than the other tests.

Horton's [1940] equation was derived based on the assumption that exhaustion processes are involved in the reduction of the infiltration rate as the test proceeds. In such processes the rate of performing work is proportional to the amount of work remaining to be performed. In general, for a ponded infiltration test conducted in a partially saturated medium the pressure gradient affecting the flow rate depends on both the height of ponding and the magnitude of the natural state capillary pressure. As the wetting front moves downward, the pressure gradient decreases and accordingly so does the infiltration rate. Eventually, the front moves far enough away so that the pressure gradient becomes negligible compared to the gravity force and infiltration rate becomes steady. Infiltration rate would continue to decrease if the infiltrating water moved from high- to low-permeability regions. Strongly heterogeneous media (even those without a systematic depth trend in permeability) tend to show a greater decrease in infiltration rate with time than do homogeneous media, as large high-permeability flow paths that are accessible from the ground surface fill rapidly, leading to a large initial infiltration rate. Another mechanism for a decreasing infiltration rate that has been demonstrated for soils is the redistribution of entrapped air above the wetting front [*Faybishenko*, 1999a].

Under ponded conditions in fractured basalt the exhaustion processes leading to a decrease in infiltration rate include surface and fracture sealing due to in washing, swelling of colloids, redistribution of particles, and microbiological clogging. However, numerical simulations of the Box Canyon infiltration test [*Doughty*, this issue] showed a significant decrease in the infiltration rate during ponding even without taking into account exhaustion processes. We assume that in addition to near-surface fracture sealing, the infiltration rate also decreases due to the following processes:

1. As water fills the highest-permeability vesicular basalt and closely spaced fractures in the upper part of the basalt flow, it is funneled to the lower-permeability, widely spaced fractures in the massive basalt in the lower part of the basalt flow, and the overall permeability decreases as the test proceeds.

2. As water moves into partially saturated fractures and imbibes into the matrix, the air it replaces may redistribute itself and block liquid flow paths [*Faybishenko*, 1995; *Persoff and Pruess*, 1995]. During the first 6–7 days of the 1996 test and

Table 3. Summary of Parameters Obtained by Fitting Horton's Equation (1) to Cumulative Infiltration Data[a]

	Tests						
Parameter	96-1	96-1	97-1	97-2	97-3	97-4	97-4
Duration, days	11	2	2	2	2	2	4
β, 1/d	0.17	0.12	1.32	4.02	1.17	0.21	0.21
i_0, cm/d	11.01	10.23	9.96	17.70	6.74	4.05	4.16
i_f, cm/d	0.00	4.72	2.16	2.70	1.63	3.01	0.63

[a]Note that in 1996, the test was completed in 14 days, whereas the first three tests in 1997 lasted 2 days, and the fourth test lasted 4 days.

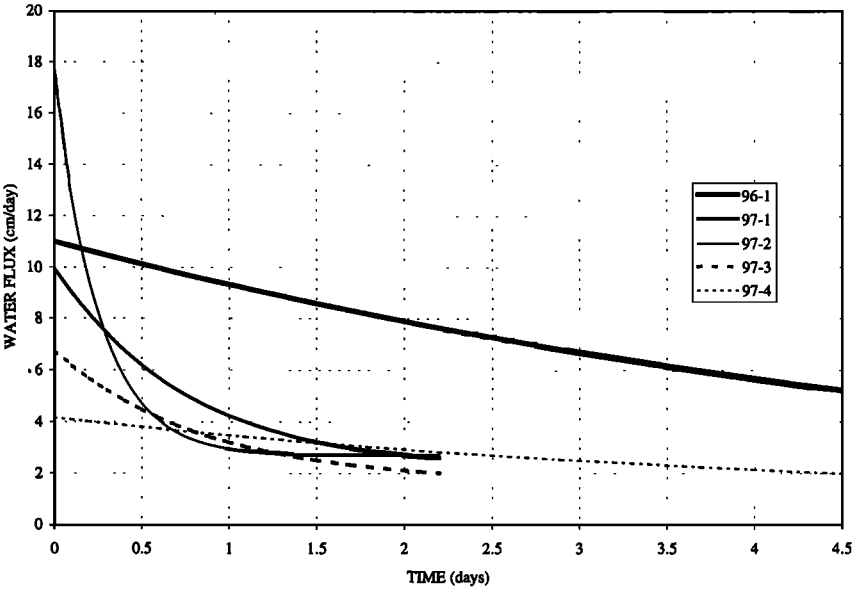

Figure 7. Time variation of the infiltration rates as determined from the derivative of the cumulative infiltration curves using equation (2).

during the 1997 tests, air bubbles were observed rising to the surface at several locations within the pond.

The infiltration rate V (cm/d) into the subsurface is obtained by differentiating (1) [*Jury et al.*, 1991]:

$$v = dq/dt = i_f + (i_0 - i_f) \exp(-\beta t). \quad (2)$$

Infiltration rates as determined from (2) are shown in Figure 7, and the fitting parameters are given in Table 3. Although the initial water depths in the pond were the same for all the tests (spatial average of 23 cm), initial infiltration rates varied from 4.1 cm/d (4.75×10^{-7} m/s) to 17.7 cm/d (2.05×10^{-6} m/s). During test 96-1 the water level was held constant, while during the tests in 1997 the water level dropped 4–6 cm/d. Despite these differences, the final flow rates for all tests converged to a narrow range from 1.6 to 3.0 cm/d (1.85×10^{-7} to 3.5×10^{-7} m/s). Note that the entire pond surface was water-covered throughout the tests to prevent air from entering the subsurface during infiltration tests. The decrease in infiltration rate with time observed in these tests is consistent with the results of many infiltration tests in soils [*Jury et al.*, 1991] and fractured rocks [*Kilbury et al.*, 1986], in which a similar pattern of decreasing infiltration rate was observed.

Detailed analysis of the infiltration rate (Figure 6 and Table 4) indicated that the measured cumulative infiltration exhibited short-term fluctuations, which increased in magnitude with each successive surface flooding. For example, Figure 6 shows that despite the overall trend of a decrease in the infiltration rate in test 97-4, at 0.7 days the infiltration rate rapidly increased, followed by a period of 0.3 days when the infiltration rate was practically zero; significant fluctuations were also observed from 1.6 to 1.9 days. Table 4 shows that for each successive test, the standard error increases and the correlation coefficient decreases for the experimental data fitted to Horton's equation. This analysis indicates that the infiltration rate decrease is less gradual (i.e., more pulse-like) with each successive pulse. These findings are consistent with those of *Vandevivere et al.* [1995], who observed that during infiltration tests in soils with microbiological clogging, hydraulic conductivity may not decrease monotonically but with fluctuations.

During test 96-1, local infiltration rates were measured with nine infiltrometers (25 cm diameter) within the pond. The water level within the infiltrometers was maintained at the same level as in the pond. The infiltration rates were mostly within the same range as the overall pond infiltration rate, as shown in Table 5. The smallest flux value (infiltrometer 4) was

Table 4. Standard Error and Correlation Coefficients Determined by Fitting Horton's Cumulative Infiltration Function to Data Collected in the Field During the Four Infiltration Tests in 1997

Test	Standard Error	Correlation Coefficient
97-1	0.047	0.9998
97-2	0.083	0.9988
97-3	0.102	0.9962
97-4	0.206	0.9942

Table 5. Flow Rates Calculated for Individual Infiltrometers and the Entire Pond for September 2–4, 1996[a]

Infiltrometer	Average Flow Rate, cm/d	Description of Surface
1	3.3	soils (2.5 cm)
2	3.6	soils (5 cm) and cracks
3	3.2	soils (5 cm) and cracks
4	0.4	dense basalt
5	1.7	soils (5–15 cm)
6	2.4	soils (30 cm)
7	3.3	soils (15–20 cm)
8	2.4	soils (10–15 cm)
9	1.8	dense basalt
Pond volume averaged	3.1	

[a]Note that these data were calculated using the water level drop at night when evaporation was practically negligible.

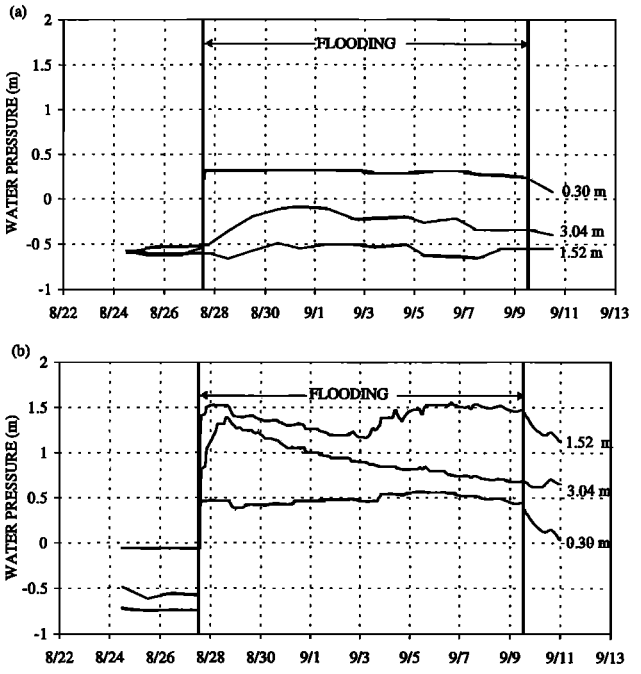

Figure 8. Time trend of water pressure measured with tensiometers in boreholes at different depths before and during test 96-1: (a) well T-5 and (b) well T-9. Note that daily averaged pressures are shown before the test and in well T-5 during the test at depths of 1.52 and 3.04 m because pressure fluctuations were large due to temperature fluctuations. Otherwise, nine-point averaged pressures are shown.

measured at a location where the infiltrometer was installed on the top of a basalt column. Calculations using the water flux and hydraulic gradients in a near-surface 30–60 cm zone showed the range of hydraulic conductivity from 0.003 m/d (3.5×10^{-8} m/s) to 0.9 m/d (10^{-5} m/s), with the lowest values associated with the vesicular basalt and the largest values associated with fractures.

5.2.2. Water pressure. In this section we analyze the results of field measurements of water pressure using tensiometers from test 96-1 and test 97-3. Measurements were taken at 23 locations between depths of 0.3 and 3 m in eight wells within the pond and three wells outside the pond. Figure 8 shows typical results of water pressure measurements in two boreholes located within the pond. Figure 8a shows that in well T-5 a gradual response at a depth of 3.04 m underlies no arrival at a depth of 1.52 m, indicating the phenomena of bypass and nonuniform vertical flow. Figure 8b shows that in well T-9 the water pressure decreased after the initial rapid increase at depths of 1.52 and 3.04 m. At a depth of 1.52 m the water pressure increased again after 7 days. Thus, during test 96-1 a steady state regime of hydraulic heads did not develop below 0.3 m.

In contrast to the almost instantaneous response of tensiometers to the beginning of ponding, the pressure responses after the end of ponding occurred more slowly. *Finsterle and Faybishenko* [1999] and *Faybishenko and Finsterle* [2000] used the results of a laboratory test and numerical modeling of the saturation-desaturation of a fractured basalt core to show that the water pressure measured in fractured rocks by tensiometers is determined by the most permeable component (fracture or matrix) at the time of measurements. Their studies revealed that during the saturation event the tensiometer measures the fracture water pressure and during the drying event it measures the matrix water pressure.

A summary of the changes in water pressure that occurred during tests 96-1 and 97-3 is given in Table 6 for three depth intervals:

1. In the shallow interval (0.3–0.6 m), all the tensiometers showed rapid pressure increases (within 0.5–1 day) during test 96-1, and five of the eight probes showed rapid increases during test 97-3. The three probes that showed no response were already in a wetted formation (indicated by a positive pressure) before the start of test 97-3. They showed no response because under wetted conditions, the arrival of infiltrating water is not necessarily accompanied by a notable pressure increase.
2. In the intermediate interval (1.5–1.8 m), during both tests, some tensiometers responded gradually (within 1–3 days) to ponding, suggesting slow, indirect routes of water travel.
3. In the deep interval (2.7–3 m), there were very few rapid arrivals and a larger number of nonarrivals, indicating that water bypassed most of the tensiometers.

These observations are consistent with the structure of the fracture pattern observed within a single basalt flow, which showed a tributary structure that funnels flow from many shallow fractures to a few fractures as depth increases, as shown in Plate 1 and Figure 5. Figure 9a shows that lithology at the tensiometer location does not correlate well to water arrival time. This is because arrival time depends on the entire flow path above and below the probe.

Some examples of the vertical hydraulic head profiles determined prior to and during tests 96-1 and 97-3 are shown in Figure 10. If the hydraulic head profile is located to the right of the diagonal (solid line), the water pressure is positive, and the hydraulic system is saturated or quasi-saturated (with entrapped air). If the hydraulic head profile is located to the left of the diagonal, the water pressure is negative, and the system is unsaturated. In well T-5 during test 96-1 (Figure 10a), the saturated (or quasi-saturated with entrapped air) zone extended from the surface to a depth of ~0.6 m, and the unsaturated zone was present below this depth. However, in the same well during test 97-3 the unsaturated zone extended all the way to the surface (Figure 10b), although conditions were generally wetter in 1997. In well T-9 the formation was saturated (or quasi-saturated) during test 96-1 from the surface to 3 m (Figure 10c), but in test 97-3, there was an unsaturated

Table 6. Categorization of Tensiometer Responses by Depth for the 1996 Test

Depth Intervals, m	Response				Saturated Before Test
	Rapid	Gradual	None	Total	
		Test 96-1			
0.3–0.6	8	0	0	8	1
1.5–1.8	4	3	1	8	1
2.7–3.0	3	2	2	7	1
Total	15	5	3	23	3
		Test 97-3[a]			
0.3–0.6	5	0	3	8	4
1.5–1.8	1	3	4	8	2
2.7–3.0	1	1	5	7	1
Total	7	4	12	23	7

[a]Pressure data from the third test were used because the data records from the other pulses were incomplete due to technical problems with the data acquisition system.

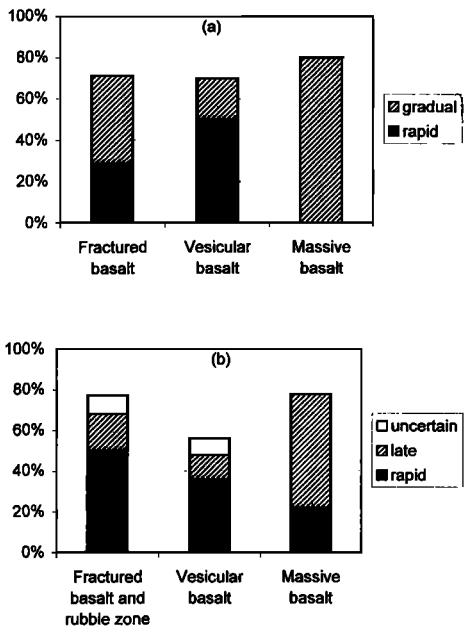

Figure 9. Correlations between lithology and water arrival times: (a) tensiometer measurements and (b) water sampling by suction lysimeters.

zone near the surface (Figure 10d). The presence of a saturated zone determined by a local measurement does not necessarily reflect the overall wetted condition beneath the pond.

5.2.3. Changes in moisture regime. Changes in the moisture regime were determined using neutron logging, time domain reflectometry (TDR), and ground-penetrating radar (GPR). It appears that the absolute value of the moisture content in fractured rocks cannot be determined from field measurements using these techniques because it is difficult, if not impossible, to obtain calibration curves for fractured rocks [*Bishop and Porro*, 1996]. Therefore we interpret relative increases in neutron counts and electromagnetic wave travel times as identifying zones of increased moisture content and use them to locate zones of preferential flow.

On the basis of neutron logging, numerous local increases in moisture content were observed during test 96-1, particularly at depths of 3 to 4 m and 6.5 to 10 m (Figure 11). These local moisture content increases indicate preferential flow paths with water bypassing locations above, between, and below these locations. Well R-3, whose neutron logging data are presented in Figure 11, is a slanted well drilled from the outside of the pond that intersects the vertical projection of the pond at a depth of 12.2 m. The moisture increases above this depth indicate horizontal flow beneath and beyond the infiltration pond. The moisture profiles in this deep slanted well prior to and during the tests in 1997 were almost identical to the moisture profiles at the end of test 96-1. Apparently, the formation was wetted during test 96-1 and did not return to background conditions 1 year later, before the beginning of test 97-1.

Neutron logging of well T-10 showed that a 1-m zone beneath the pond and a low-angle fracture at 1.5 m were wetted sometime during the 1997 tests, while no moisture increase occurred below that depth (Figure 12a). The moisture content at the depth of 1.5 m rapidly increased sometime between tests 97-1 (ended on September 13, 1997) and 97-2 (started on September 18, 1997), and then increased slowly thereafter (Figure 12b).

Plate 3a shows a wave velocity difference tomogram, obtained using GPR surveys conducted between wells R-1 and R-2 prior to and during test 96-1. There were several local increases in moisture content, especially within the central fractured zone and the rubble zone. During tests 97-1 and 97-2, no significant changes in the moisture content were observed using GPR.

TDR probes were installed near the surface to a depth of 0.5 m. All probes within the pond responded almost immediately to ponding, indicating a rapid saturation of both the fractures and matrix at depths down to 0.5 m. These measurements suggested that the near-surface weathered basalt acted

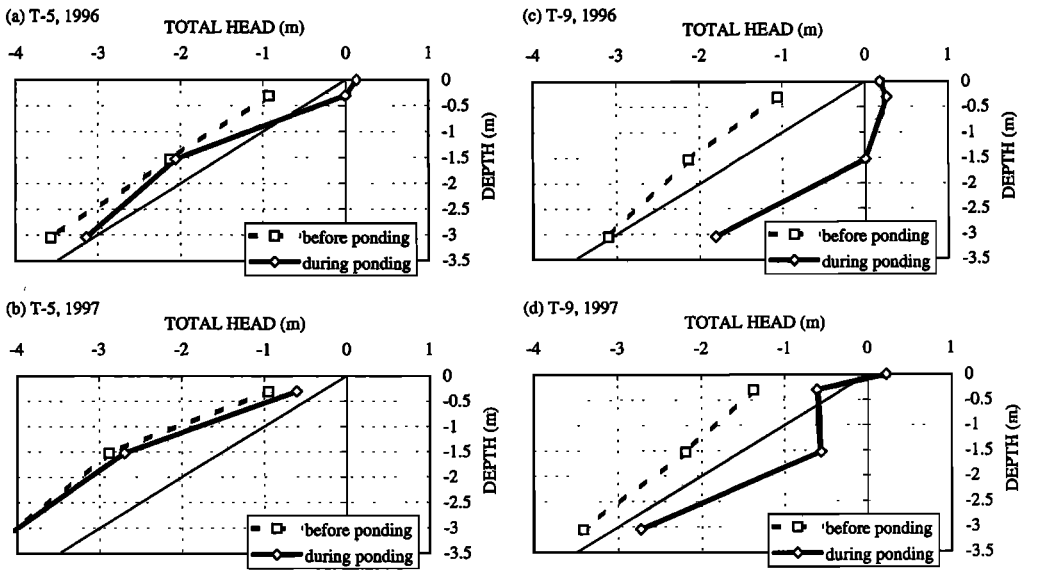

Figure 10. Hydraulic head variations with depth in wells T-5 and T-9 before and during the infiltration tests: (a) well T-5, test 96-1; (b) well T-5, test 97-3; (c) well T-9, test 96-1; and (d) well T-9, test 97-3.

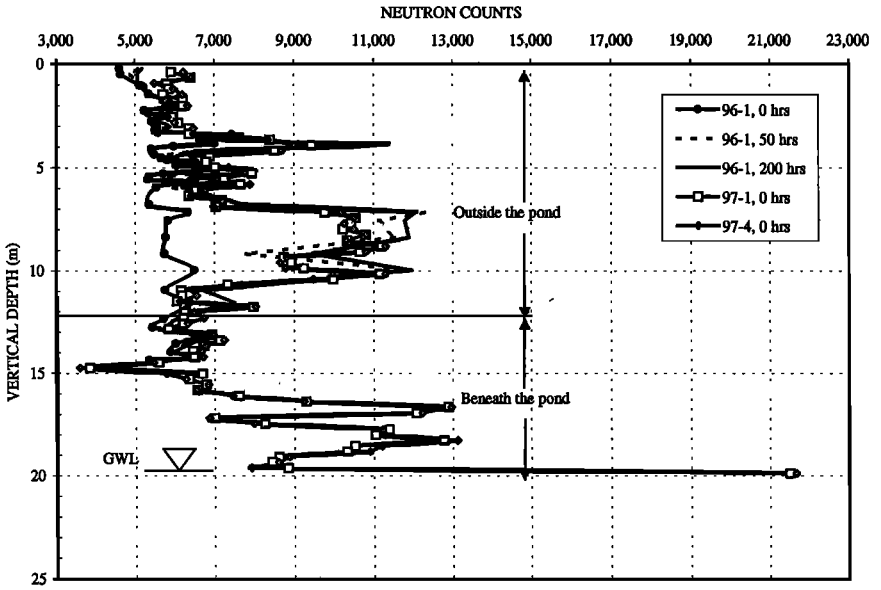

Figure 11. Neutron logging results in well R-3, a slanted borehole located partially (from the surface to the depth of 12.2 m) outside of the pond and partially beneath the pond before and during test 96-1 and the tests in 1997. Note that the groundwater level is at 19.8 m. An increase in neutron counts is interpreted as an increase in moisture content.

as a porous medium. Probes located outside the pond responded later during the infiltration test, indicating lateral movement of water in the near-surface zone.

5.2.4. Temperature. Subsurface temperature changes may arise via two modes of heat transfer from the ground surface: conduction caused by temperature gradients and convection caused by infiltrating water. In a homogeneous medium, temperature changes due to conductive heat transfer with a periodically varying surface temperature are dampened exponentially with depth and delayed in time. Using subsurface temperature profiles collected from Box Canyon [*Long et al.*, 1995], conduction theory predicted that daily temperature variations could propagate only ~0.5 m, while seasonal temperature variations could propagate to a depth of 10 m. Departures

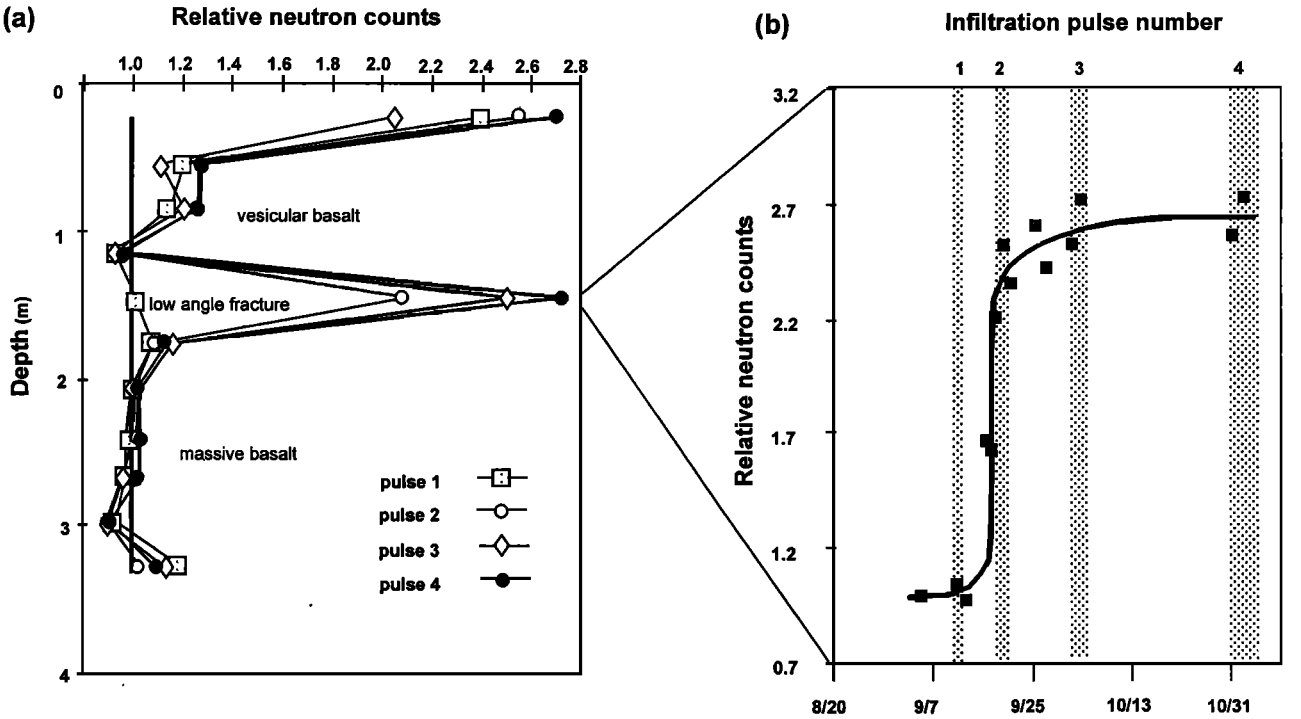

Figure 12. Neutron counts relative to pretest counts in well T-10, a vertical borehole located inside the pond, during the 1997 tests: (a) vertical profile and (b) temporal change at 1.5 m. The width of the shaded area indicates the duration of the infiltration test.

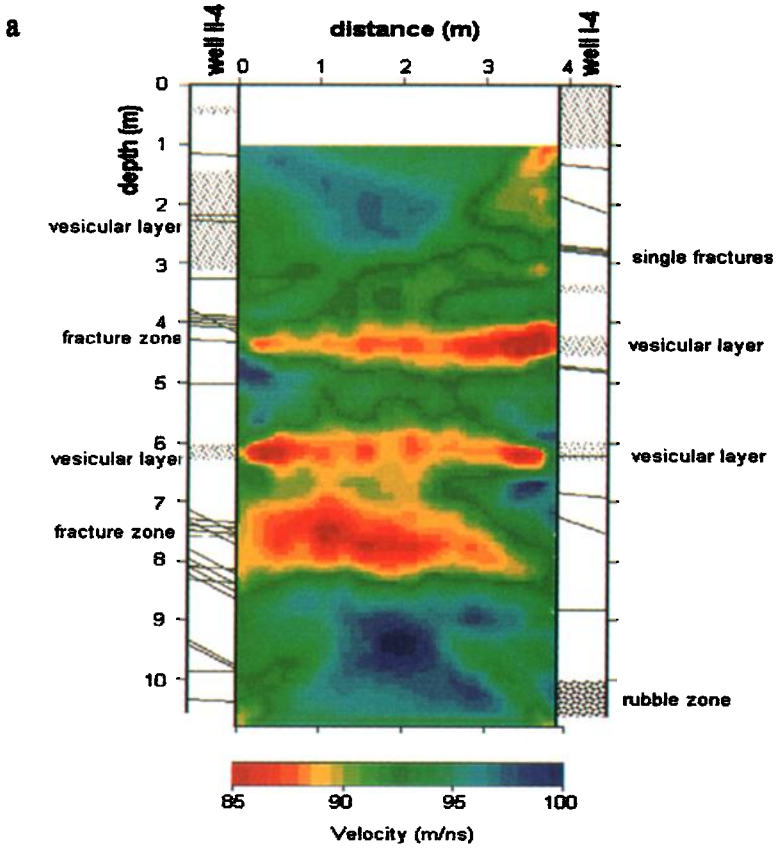

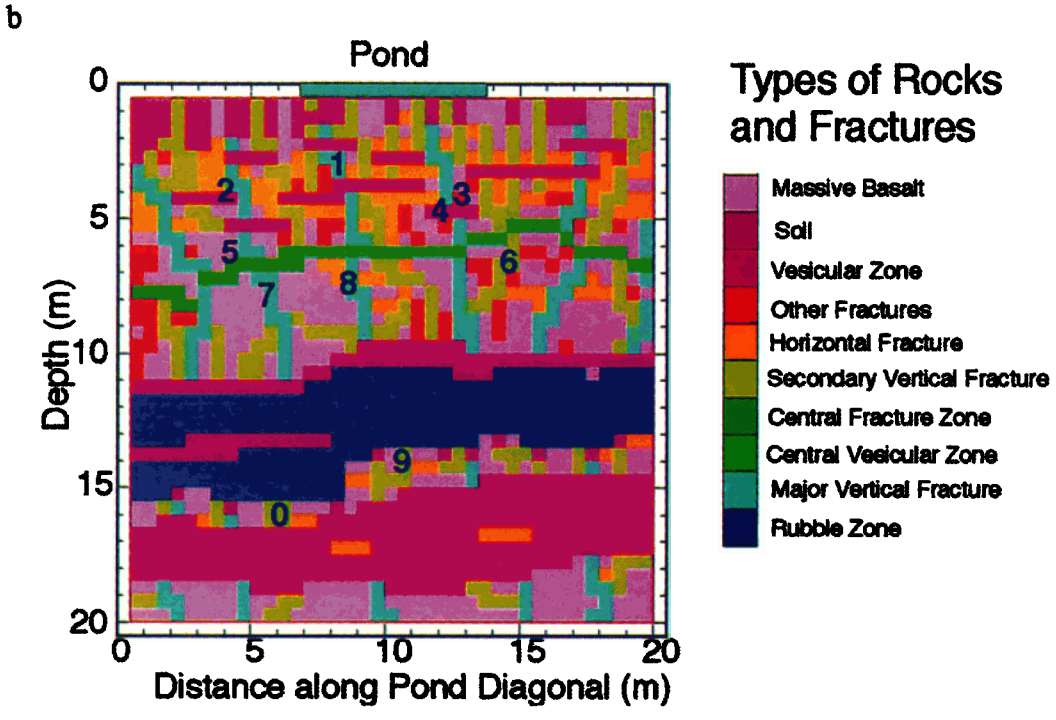

Plate 3. (a) A wave velocity difference tomogram obtained from GPR surveys conducted prior to and during test 96-1. Note that a decrease in velocity, which is represented by the red and yellow areas, is interpreted as an increase in the moisture content [*Hubbard et al.*, 1997; *Peterson et al.*, 1997; *Vasco et al.*, 1997]. (b) Numerical 2-D modeling of transport of a conservative tracer during ponded infiltration at the Box Canyon site showing classification of rocks and soils. Locations 0 and 9 showed a insignificant increase in concentration after 17 days.

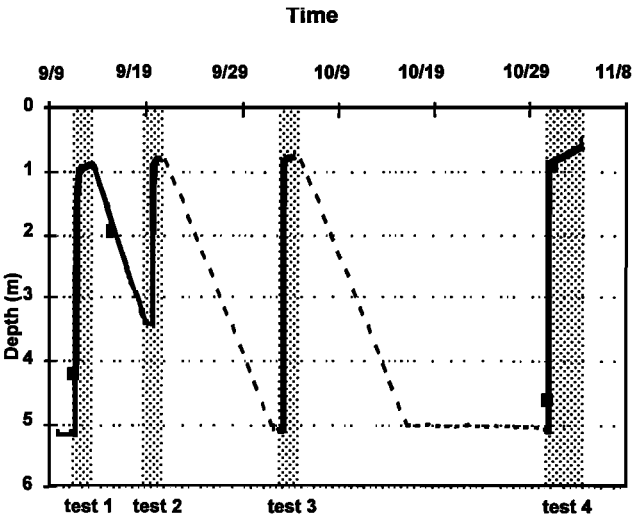

Figure 13. Water level in well I-5 during the 1997 tests. The shaded areas indicate the time during which the surface was ponded.

from this general pattern indicate that convection is altering the temperature profile and potentially could be used to locate preferential flow paths.

During test 96-1, subsurface temperature measurements were for the most part consistent with purely conductive heat flow: temperature changes generally decreased with increasing depth and no thermistor deeper than 7 m showed any temperature change. Of the 29 thermistors used to conduct measurements, seven showed changes in temperature that could not be explained by conduction alone. Six of the seven were gradual changes in temperature that differed from conduction theory by at most a few degrees. The strongest evidence for convective flow occurred at a depth of 4.6 m in well I-3, where the temperature response showed small daily temperature variations at a depth far too great to be explained by conduction, strongly suggesting that a fast flow path for infiltration was nearby. During the tests in 1997, all the temperature observations were consistent with conductive heat flow, probably because of the smaller volume of water infiltrated and the wetter pretest conditions, both of which factors would lessen the thermal signature of the infiltrating water.

5.2.5. Perched water levels. Observations using tensiometers installed in backfilled boreholes showed that at some locations the water pressure became positive (0.15–1.85 m) during ponding, indicating that local perched water zones were formed because of infiltration. Perched water zones were also identified in cased, but open at the bottom boreholes within the footprint of the pond. For example, the height of water above the bottom of well T-10 (depth 3.05 m) was 0.65 m, and it was 0.35 m in well T-8A (depth 6.1 m). During test 96-1, seepage of water was observed along the borehole wall at the level of the rubble zone (~12 m depth) in wells II-7 and II-2. Water also accumulated at the bottom of well II-6 at a depth of 12 m. Wells II-2, II-6, and II-7 are open, uncased wells located 3–5 m NW, east, and SE, respectively, from the infiltration pond (see Plate 2a). However, not all of the open wells outside the pond showed perched water at the rubble zone depth, indicating that lateral flow was not uniformity distributed away from the infiltration pond.

During the tests in 1997, perched water was observed in well I-5 (a 12-m-deep well located 1.5 m from the boundary of the pond) with an almost immediate rise in the water level during ponding and then a dramatic drop during periods of drying (Figure 13). This indicates that there was a major fast flow path linking the pond with the borehole. Note that transient water level changes in conventional boreholes installed in fractured rocks are not quantitative indicators of in situ conditions because of the different specific yield (S) for the fractured rock ($S \ll 1$) and the open space ($S = 1$) of a borehole. Thus our water level observations confirmed that open, uncased boreholes in fractured rocks could lead to misleading results because of short-circuiting between otherwise unconnected fractures.

5.2.6. Water and tracer sampling. During the first week of test 96-1 (before the tracer was added), water samples were taken to determine the water arrival time at different depths. Table 7 shows a decrease in the percentage of locations (from 82% to 44%) of water arrival with depth through the upper half of the basalt flow (down to 5 m), which is presumably due to the increase in fracture spacing with depth. These data are consistent with the tensiometer data (Table 6) and support the hypothesis of a funneling of flow with increasing depth. There is an increase in the percentage of locations showing water arrival near the central fracture zone (73% within the 5 to 9 m interval) and rubble zone (67% within the 9 to 14 m interval) because these zones allow both lateral and vertical flow to occur more easily. The first arrival times given in Table 7 show rapid movement of water, of the order of 5 m/d (6×10^{-5} m/s) through the fastest flow paths. However, there were locations at every depth that did not respond during the test.

Figure 9b illustrates that the percentage of rapid arrivals was higher at locations of fractures and rubbles and lower in the massive basalt and the percent of late arrivals does not correlate to lithology. Whether or not water arrives to a certain location depends on the entire pathway from the ground surface to the space around the lysimeter. Early arrivals are interpreted as reflecting a relatively direct pathway from the surface to the monitoring location along fractures. Additionally, the suction lysimeter is not a point-type probe because as vacuum is applied, water is drawn from a certain rock volume around the probe. Once the moisture content of fractures and matrix changes, the radius of influence changes as well.

The tracer arrival data from test 96-1 were consistent with water sampling and tensiometry data, suggesting that no single tracer front moved uniformly downward during infiltration, reinforcing the hypothesis of preferential water flow. The tracer was detected in lysimeters installed in the rubble zone at

Table 7. Categorization of Water Arrival Time by Depth Using Suction Lysimeter Data for the 1996 Test

Depth Intervals, m	Number of Locations Where Water Arrived[a]	Total Number of Locations Sampled	Percent of Locations Showing Water Arrival	First Arrival Time, days since start of test
0–1	9	11	82	<1
1–2	7	10	70	<1
2–3	6	9	67	<1
3–5	4	9	44	<1
5–9	8	11	73	1
9–14	4	6	67	2
Total	38	56	68	

[a]During 11 days of monitoring.

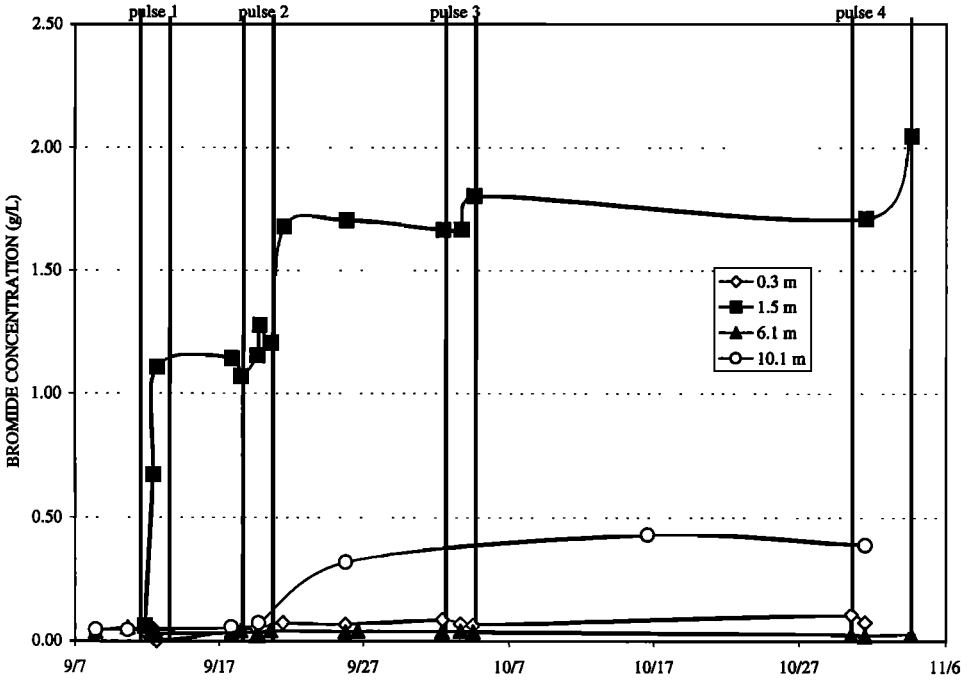

Figure 14. Breakthrough curves for bromide during the 1997 tests for well I-1 at four depths (0.3, 1.5, 6.1, and 10.1 m). Vertical lines show the duration of pulses. Note that well I-1 is a vertical borehole within the boundaries of the pond.

depths of 10.5 and 12 m and in the fracture zones (or individual fractures) at depths of 2.6, 5.5, 7.2, and 10.1 m.

Tracer data from the tests in 1997 were for the most part consistent with tracer data from test 96-1. Figure 14 illustrates breakthrough curves for bromide obtained at different depths in well I-1. The wetter conditions and larger mass of tracer introduced during these tests (see Table 2) allowed the tracer to penetrate deeper into the formation than during test 96-1. At a depth of 1.5 m, bromide concentrations reached over 2 g/L, whereas at 0.3 m, located directly above this point, the concentrations remained at background levels (<0.05 g/L), showing strong evidence of preferential flow. A tracer concentration of 0.43 g/L was detected at a depth of 10.1 m, where a horizontal fracture/rubble zone was identified in the lithological log (see Plate 2a).

5.2.7. Electrical resistivity. Miniature electrical resistivity (ER) probes were used to determine localized resistivity values along the boreholes during the infiltration tests. Temporal variations occurred in all tests, usually with decreases in resistivity during ponding (Figure 15a), which we interpret as an increase in tracer (salt) concentration. In general, resistivity values were lower during the tests in 1997 than during test 96-1 because the formation was wetter and/or more saline after the 1996 infiltration test. These results are in agreement with the data obtained from neutron logging, GPR, and tensiometry data.

Nearly all the ER probes (96%) located near fractures or in the central fracture zone showed a decrease in resistivity during the tests in 1997, indicating that the tracer eventually reached most if not all fractures (Figure 15b). Half the probes in the rubble zone (~12 m depth), 33% of the probes in vesicular basalt, and 30% of the probes in massive basalt showed a decrease in resistivity. Thus the ER measurements showed a qualitative correlation to lithology.

5.3. Insights From Numerical Modeling of the Ponded Infiltration Test

Numerical modeling was used as a tool to investigate the effects of fracture geometry, lithology, and entrapped air (which cannot be monitored in detail under field conditions) on water and air velocity fields, infiltration rate, and tracer breakthrough curves. Here we summarize insights into the conceptual model of flow and transport gained from the two-dimensional (2-D) (vertical plane) numerical model of test 96-1, described in detail by *Doughty* [this issue]. The spatial discretization for the 2-D model (Plate 3b) was created based on the geometry of the fracture pattern and lithology of the exposed Box Canyon cliff face (Plate 1) as well as on borehole lithological data.

Modeling results suggest that the infiltration rate is sensitive to both the intrinsic permeability of the highest-permeability features (column-bounding fractures, denoted as primary vertical fractures in Plate 3b) and the functional form of the relative permeability curves used. Despite the fact that the model did not explicitly include a temporal decrease in the hydraulic conductivity of the near-surface layer (see section 5.2), it showed a significant temporal decrease in the infiltration rate. Modeling results suggest that coupled effects of the geometry of flow (resulting in the funneling effect), the overall decrease in the rock permeability with depth, and entrapped air contribute to the decrease in infiltration rate.

The model predicted an irregular pattern of flow through the subsurface during the ponded infiltration test, with much of the water flow occurring preferentially through the highest permeability vertical fractures. Short-range lateral flow occurred through vesicular lenses, the central fracture zone, and the rubble zone. Simulation of tracer movement showed a variety of breakthrough curves in fractured basalt (Figure 16)

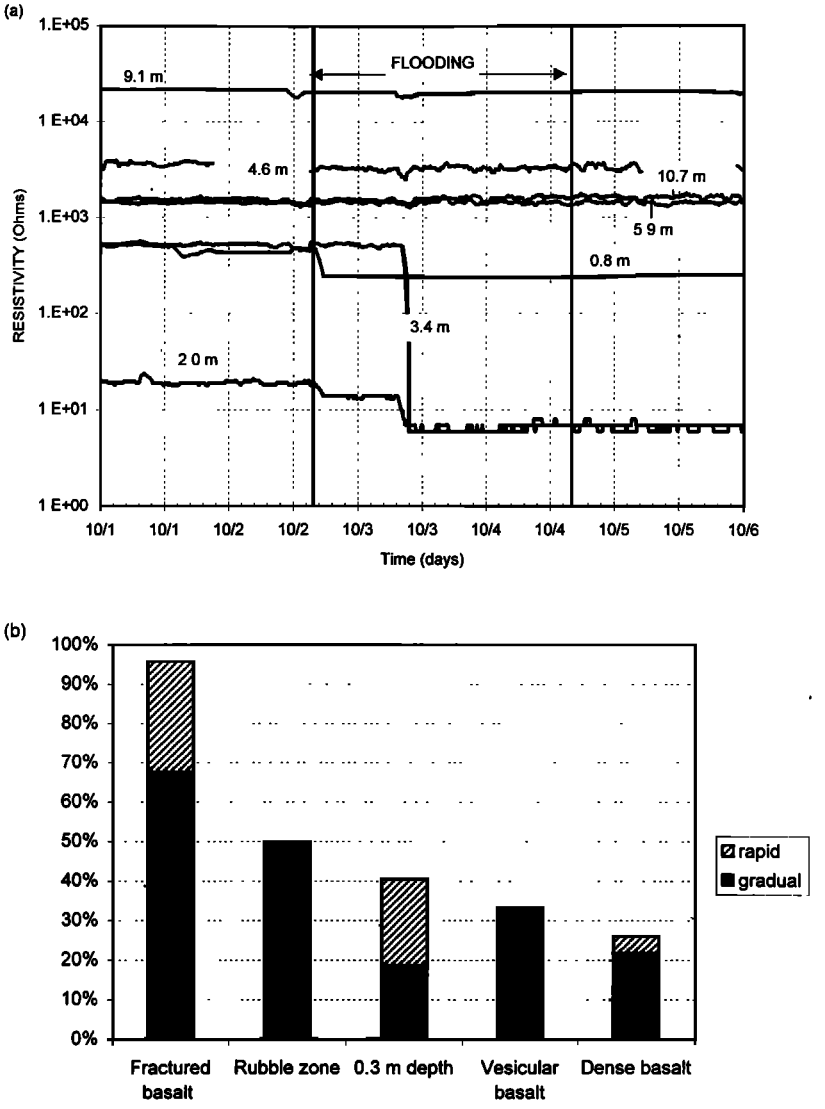

Figure 15. Results of ER probe measurements: (a) example of temporal ER response in well S-3 during test 97-3 showing the decrease in electrical resistivity as affected by the tracer at depths of 0.8, 2.0 and 3.4 m and (b) classification of all ER probe measurements made during the 1997 tests according to lithology.

confirming the results of both the LSIT (Figure 3) and the Box Canyon infiltration tests (Figure 14). Plate 3b shows that two probes located next to each other (e.g., locations 3 and 4), but representing different flow paths, generate different breakthrough curves.

The modeling studies considered two treatments for the air present in the vadose zone [*Doughty*, this issue]. In the first case, using the traditional soil physics approach, air was treated as a passive phase, and the model only simulated water flow. In the second case, the vadose zone was considered as a two-phase flow system, in which coupled water and air flow were simulated. The results suggested that air flow and entrapped air significantly affect infiltration, creating a more nonuniform moisture distribution in the subsurface and decreasing the infiltration rate by ~30%. Examination of gas-phase flow paths showed that while much of the air was purged from the subsurface region below the pond via lateral flow through the central fracture zone and rubble zone, some air became entrapped and subsequently flowed upward into the pond through the column-bounding fractures.

6. Summary of the Conceptual Model of Water Flow

The data obtained during the infiltration tests have confirmed that infiltration is primarily controlled by the characteristics of the fracture system within the basalt flow, leading to strongly preferential, irregular, and nonrepeatable flow patterns in the subsurface. Comparisons between test 96-1 and the tests in 1997 show that flow patterns and zones of saturation are highly variable from test to test. Apparently, they do not depend solely on lithological features but are sensitive to both initial conditions and flow history. Beneath the pond, the basalt may be found in unsaturated, saturated, and quasi-saturated conditions with entrapped air. These phenomena confirm the complex character of water flow in a fractured basalt vadose zone over space and time.

In order to describe such a complex system we propose the multi-geological-component conceptual model illustrated in Figure 17. This conceptual model recognizes the connections between individual geological components, each with different

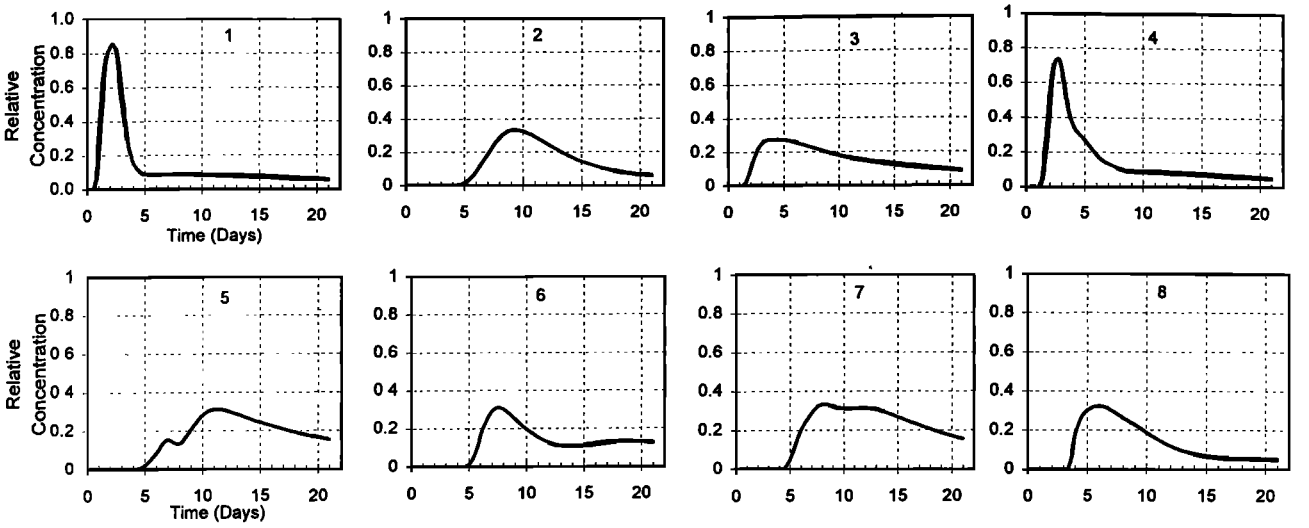

Figure 16. Breakthrough curves corresponding to numbered locations in Plate 3b.

hydraulic processes governing water flow. Figure 17 shows the main processes of water flow: preferential flow through conductive vertical fractures, fracture-to-matrix diffusion, vesicular basalt-to-massive basalt diffusion, the funneling effect, and lateral flow (with advective transport) through subhorizontal fractures and rubble zones. This multi-geological-component conceptual model is far more complicated than most existing conceptual models for fractured/porous media, such as double-porosity [*Barenblatt et al.*, 1960; *Warren and Root*, 1963] or triple-porosity [*Abdassah and Ershaghi*, 1986] models. The simpler models cannot account for all the processes necessary to make accurate predictions of flow and transport in the fractured basalt vadose zone. The key features of our conceptual model are summarized in the following paragraphs.

Pressure measurements and TDR measurements indicated that wetting of the top 0.5 m zone beneath the pond occurred very rapidly. Preferential flow appeared to originate just below this depth, and flow became increasingly localized with increasing depth, as evidenced by the successively fewer instruments responding to ponding. The tree structure of the fracture pattern conceptualized in Figure 5 is consistent with the concept of flow funneling. Multimodal breakthrough curves that were obtained at the LSIT, the Box Canyon infiltration tests, and using numerical modeling provide further evidence of a confluence of water flow through different sets of fractures of varying permeability and geometry. In this conceptualization, column-bounding fractures provide the primary pathways for fast vertical infiltration. However, the water supply from the surface into column-bounding fractures is restricted due to limited infiltration through sediments filling near-surface fractures. Some fractures terminate within the basalt flow, either creating dead-end flow paths or indirect flow paths composed of linked column-normal and column-bounding fractures. Furthermore, we expect that water flow within initially dry fractures will show the fingering phenomena that have been identified at the laboratory scale [*Nicholl et al.*, 1994; *Geller et al.*, 1996; *Glass and Nicholl*, 1996] and in modeling studies [*Pruess*, 1999], so even conductive column-bounding fractures will not be uniformly wet. Thus simply identifying a monitoring point as being located in a vertical fracture does not enable one to

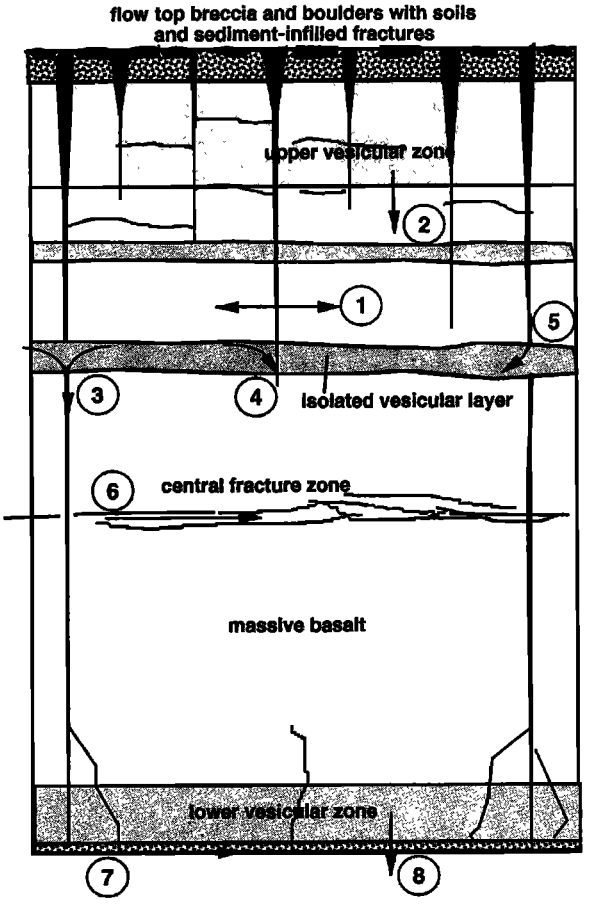

Figure 17. A conceptual model of mechanisms of water flow in a multi-geological-component system representing fractured basalt: (1) fracture-to-matrix diffusion, (2) vesicular basalt-to-massive basalt diffusion, (3) preferential flow through conductive fractures and the effect of funneling, (4) vesicular basalt-to-nonconductive fracture diffusion, (5) conductive fracture-to-vesicular basalt flow and diffusion, (6) lateral flow and advective transport in the central fracture zone, (7) lateral flow and advective transport in the rubble zone, and (8) flow into the underlying basalt flow.

predict the flow response because the response at any point depends on the entire flow path both above the monitoring point and below the monitoring point for nonconductive, dead-end fractures.

Since the largest fractures are vertical, the predominant flow direction under gravity is downward. However, geological features such as the horizontal fractures connecting terminated vertical fractures, the vesicular lenses, the central fracture zone, and the rubble zone promote lateral flow. If the permeability below the rubble zone is low (likely if the underlying fractures were exposed at the surface for a period of time and are consequently sediment filled) or if a sedimentary interbed occurs there (as at the LSIT, which is typical for the INEEL area), perched water zones can be created and lateral flow can be widespread. Given the high porosity of the rubble zones (presumably up to 50% or higher), the potential for storage and movement of water (and consequently contaminants) is large. Once positive hydraulic pressure is developed within the perched water in the rubble zone, water may migrate upward into dead-end fractures in the lower part of the basalt flow (see Plate 1 and Figure 5), and then from there can be imbibed into the matrix.

The decrease in infiltration rate with time observed in all tests is consistent with the theory and experience of infiltration from the land surface [*Jury et al.*, 1991]. We hypothesize that the main factors affecting the infiltration rate are the topsoil layer, the interface between the soil layer and the fractured basalt, and the near-surface soil-infilled fractures. Small variations of these factors may cause the large range of initial infiltration rates for the tests. Another example of sensitive dependence on local conditions may be the tendency for a pulse-like infiltration rate that was observed during test 97-4. We hypothesize that water penetrates into horizontal fractures only if a critical hydraulic pressure is reached, at which point a hydraulic connection between column-bounding fractures is established. Once a hydraulic connection is made, water begins to flow through the fracture producing a rapid, but short-term increase in the infiltration rate, despite its long-term decreasing trend.

Numerical modeling suggests that the presence of air has a significant effect on infiltration rate and subsurface saturation distribution, and the observation of air bubbles rising through the pond confirms that entrapment of air does occur. We hypothesize that entrapment of air within the wetted zone beneath the pond occurred in both the vesicular basalt and the fractures infilled with sedimentary material due to the irregular spatial flow pattern.

7. Conclusions and Future Research

The data from the intermediate-scale infiltration tests conducted at Box Canyon combined with those from the LSIT [*Newman and Dunnivant*, 1995; *Wood and Norrell*, 1996] have shown that it is impossible to identify a priori which fractures will transmit water during an infiltration test, implying that much of the monitoring network will be unused. Instruments that do respond are likely to be sparsely distributed, and their responses difficult to interpret in terms of the scale of the infiltration problem as a whole. Therefore our approach to the development of a conceptual model of water flow in a fractured basalt vadose zone is based on a combination of the lithological information and fracture pattern data together with the results of the infiltration tests. The scale of the Box Canyon experiment was chosen to be relevant to both the scale of geologic variability and the scale of contamination problems, for example, leakage from a single tank.

Even with the geology-based, relevant-scale approach we use, it is impossible to obtain a complete, integrated picture of the movement of water within the multiporosity system of massive and vesicular basalt and fractures partially infilled with sediments. Point measurements cannot be reliably interpolated for such heterogeneous systems, and geophysical measurements are not of high enough resolution to identify individual preferential flow paths. However, by using a combination of these methods, we can make the following observations. From analysis of the geological setting, we have determined that the fracture pattern exhibits a general increase in the fracture spacing downward. This fracture pattern enables a funneling of flow into progressively fewer flow paths as depth increases; such flow paths may be impossible to locate, and contaminants can move quickly through them. From analysis of the infiltration test data we find that the conventional term "water front," commonly used to characterize infiltration in sedimentary material, is irrelevant for infiltration in fractured rocks. Column-bounding fractures are the primary pathways for preferential flow from the surface toward the rubble zone at a depth of 10 to 12 m. Water flow occurs rapidly through the conducting fractures followed by a gradual saturation of the basalt matrix. Some fractures that are saturated at the beginning of the test desaturate thereafter, suggesting that steady state conditions do not develop.

The field data obtained at Box Canyon can be of general use for hydrogeologists working at other sites composed of fractured basalt and other types of fractured rocks and heterogeneous soils and can be employed to develop investigation strategies, measurement devices, and modeling approaches. For example, the data sets obtained from the Box Canyon infiltration tests were used to build confidence in numerical models used for the Yucca Mountain project [*Unger et al.*, 1999]. Moreover, such field data can be interpreted using several alternative models [*Pruess et al.*, 1999]. One exciting new area of research involves conceptualizing flow in the fractured basalt vadose zone as a chaotic dynamical system [*Faybishenko et al.*, 1998c; *Faybishenko*, 1999b]. The motivation for this approach is twofold: in the temporal regime we recognize that flow through an unsaturated fracture network may be more like a set of dripping faucets than the continuous flow predicted by Darcy's law and Richards' equation. In the spatial regime we recognize that the funneling effect of water flow through the fracture pattern, in combination with the widespread lateral flow in the rubble zone, provides the combination of chaotic processes. The important output provided by a chaotic model is information on how much can be known about the future behavior of a system. A chaotic dynamic approach may provide an entirely new paradigm for describing flow and transport behavior in the fractured basalt vadose zone [*Faybishenko et al.*, 1998c; *Faybishenko*, 1999b]. For remediation this means knowing what questions are reasonable to ask, rather than oversimplifying a system to the point of uselessness in an attempt to answer all questions.

Acknowledgments. Contributions to the design of the tests, field instrumentation, and numerous discussions with Buck Sisson, Kirk Dooley, and Tom Stoops of the INEEL and Kenzi Karasaki and others of LBNL are very much appreciated. Rohit Salve, Marque Mesa, and Ryan Nelson participated in fieldwork and preliminary data analysis.

Scott Mountford conducted analytical analyses of water samples. Ken Grossenbacher and Preston Jordan of LBNL participated in geological investigations. P. Rizzo, R. Solbau, D. Lippert, and J. Clyde participated in the design and fabrication of field instrumentation. Reviews by G. Moridis, T. Tokunaga, and J. Wang of LBNL and R. Podgorney of INEEL are very much appreciated. Thoughtful reviews of the manuscript and suggestions were given by R. J. Glass of Sandia National Laboratories and two anonymous reviewers. This work was funded by the Characterization, Monitoring, and Sensor Technology Crosscutting Program, and Environmental Management Science Program, Office of Science and Technology, Office of Environmental Management, U.S. Department of Energy (DOE) under contract DE-AC03-76SF00098. However, any opinions, findings, conclusions, or recommendations expressed herein are those of the authors and do not necessarily reflect the views of DOE.

References

Abdassah, D., and I. Ershaghi, Triple porosity systems for representing naturally fractured reservoirs, *SPE Form. Eval.*, 113–127, 1986.

Barenblatt, G. E., I. P. Zheltov, and I. N. Kochina, Basic concepts in the theory of seepage of homogeneous liquids in fissured rocks, *J. Appl. Math.*, *24*(5), 1286–1303, 1960.

Benito, P. H., P. J. Cook, B. Faybishenko, B. Freifeld, and C. Doughty, Cross-well air-injection packer tests for the assessment of pneumatic connectivity in fractured, unsaturated basalt, in *Rock Mechanics for Industry*, edited by B. Amadei et al., pp. 843–851, A. A. Balkema, Brookfield, Vt., 1999.

Bishop, C. W., and I. Porro, Comparison of neutron moisture gauges and a neutron tool for use in monitoring wells, *Ground Water*, *35*(3), 394–400, 1996.

Dahan, O., R. Nativ, E. Adar, and B. Berkowitz, A measurement system to determine water flux and solute transport through fractures in the unsaturated zone, *Ground Water*, *36*(3), 444–449, 1998.

Doughty, C., Numerical modeling of water flow in a fractured basalt vadose zone: Box Canyon site, Idaho, *Water Resour. Res.*, this issue.

Eaton, R. R., C. K. Ho, R. J. Glass, M. J. Nicholl, and B. W. Arnold, Three-dimensional modeling of flow through fractured tuff at Fran Ridge, *Rep. SAND95-1896*, Sandia Natl. Lab., Albuquerque, N. M., 1996.

Engelder, T., Joints and shear fractures in rock, in *Fracture Mechanics of Rock*, edited by B. K. Atkinson, pp. 27–69, Academic, San Diego, Calif., 1987.

Evans, D. D., and T. J. Nicholson (Eds.), *Flow and Transport Through Unsaturated Fractured Rock*, *Geophys. Monogr. Ser.*, vol. 42, AGU, Washington, D. C., 1987.

Faybishenko, B., Hydraulic behavior of quasi-saturated soils in the presence of entrapped air: Laboratory experiments, *Water Resour. Res.*, *31*(10), 2421–2435, 1995.

Faybishenko, B., Comparison of laboratory and field methods for determination of unsaturated hydraulic conductivity of soils, in *Proceedings of the International Workshop on Characterization and Measurement of the Hydraulic Properties of Unsaturated Porous Media*, edited by M. T. von Genuchten, F. J. Leij, and L. Wu, pp. 279–292, U.S. Salinity Lab., Riverside, Calif., 1999a.

Faybishenko, B., Evidence of chaotic behavior in flow through fractured rocks, and how we might use chaos theory in fractured rock hydrogeology, in *Proceedings of the International Symposium on Dynamics of Fluids in Fractured Rocks: Concepts and Recent Advances, February 10–12, 1999, Berkeley, CA, Rep. LBNL-40182*, pp. 207–212, E. O. Lawrence Berkeley Natl. Lab., Berkeley, Calif., 1999b.

Faybishenko, B., and S. Finsterle, On tensiometry in fractured rocks, in *Theory, Modeling, and Field Investigation in Hydrogeology: A Special Volume in Honor of Shlomo P. Neuman's 60th Birthday*, edited by D. Zhang and L. Winter, Geol. Soc. of Am., Boulder, Colo., in press, 2000.

Faybishenko, B., P. Holland, M. Mesa, D. Burgess, C. Knutson, and B. Sisson, Lithological conditions at Box Canyon site: Results of drilling, coring and open borehole measurements, 1995–1997 data report, *Rep. LBNL-40182*, E. O. Lawrence Berkeley Natl. Lab., Berkeley, Calif., Sept. 1998a.

Faybishenko, B., R. Salve, P. Zawislanski, K. H. Lee, P. Cook, B. Freifeld, K. Williams, and C. Doughty, Ponded infiltration test at the Box Canyon site: Data report and preliminary analysis, *Rep. LBNL-40183*, E. O. Lawrence Berkeley Natl. Lab., Berkeley, Calif., 1998b.

Faybishenko, B., et al., A chaotic-dynamical conceptual model to describe fluid flow and contaminant transport in a fractured vadose zone, *Rep. LBNL-41223*, E. O. Lawrence Berkeley Natl. Lab., Berkeley, Calif., 1998c.

Faybishenko, B., J. B. Sisson, K. Dooley, W. E. McCabe, and H. W. McCabe, New technology for borehole completion in fractured rocks using injection of polyurethane foam, *Rep. LBNL-41683*, E. O. Lawrence Berkeley Natl. Lab., Berkeley, Calif., 1998d.

Finsterle, S., and B. Faybishenko, What does a tensiometer measure in fractured rock?, in *Proceedings of the International Workshop on Characterization and Measurement of the Hydraulic Properties of Unsaturated Porous Media*, edited by M. T. van Genuchten, F. J. Leiij, and L. Wu, pp. 867–875, U.S. Salinity Lab., Riverside, Calif., 1999.

Geller, J. T., G. Su, and K. Pruess, Preliminary studies of water seepage through rough-walled fractures, *Rep. LBNL-38810*, E. O. Lawrence Berkeley Natl. Lab., Berkeley, Calif., 1996.

Glass, R. J., and M. J. Nicholl, Physics of gravity fingering of immiscible fluids within porous media: An overview of current understanding and selected complicated factors, *Geoderma*, *70*, 133–163, 1996.

Glass, R. J., T. S. Steenhuis, and J. Y. Parlange, Immiscible displacement in porous media: Stability analysis of three-dimensional, axisymmetric disturbances with application to gravity-driven wetting front instability, *Water Resour. Res.*, *27*(8), 1947–1956, 1991.

Heath, R. C., Basic ground-water hydrology, *U.S. Geol. Surv. Water Supply Pap.*, *2220*, 1984.

Horton, R. E., An approach toward a physical interpretation of infiltration-capacity, *Soil Sci. Soc. Am. Proc.*, *5*, 399–417, 1940.

Hubbard, S. S., J. E. Peterson, E. L. Majer, P. T. Zawislanski, K. H. Williams, J. Roberts, and F. Wobber, Estimation of permeable pathways and water content using tomographic radar data, *Leading Edge Explor.*, *16*(11), 1623–1628, 1997.

Jury, W. A., W. R. Gardner, and W. H. Gardner, *Soil Physics*, John Wiley, New York, 1991.

Kilbury, R. K., T. C. Rasmussen, D. D. Evans, and A. W. Warrick, Water and air intake of surface-exposed rock fractures in situ, *Water Resour. Res.*, *22*(10), 1431–1443, 1986.

Knutson, C. F., K. A. McCormick, R. P. Smith, W. R. Hackett, J. P. O'Brien, and J. C. Crocker, FY 89 report RWMC vadose zone basalt characterization, informal report prepared for the U.S. Department of Energy, Idaho Operations Office, DOE contract DE-AC07-76ID01570, EG&G Idaho, Inc., Idaho Falls, July 1990.

Knutson, C. F., D. O. Cox, K. J. Dooley, and J. B. Sisson, Characterization of low-permeability media using outcrop measurements, SPE Paper 26487 presented at 68th Annual Technical Conference and Exhibition, Soc. of Pet. Eng., Houston, Tex., Oct. 3–6, 1993.

Laubach, S. E., Fracture patterns in low-permeability-sandstone gas reservoir rocks in the Rocky Mountain region, SPE Paper 21853 presented at the Rocky Mountain Regional Meeting and Low-Permeability Reservoirs Symposium, Soc. of Pet. Eng., Denver, Colo., April 15–17, 1991.

Lee, K. H., A. Becker, B. Faybishenko, and R. Solbau, Electrical resistivity monitoring borehole array, patent application submitted to the LBNL Patent Department on 7/8/98 (IB-1425), E. O. Lawrence Berkeley Natl. Lab., Berkeley, Calif., 1998.

Lenormand, R., and C. Zarcone, Capillary fingering: Percolation and fractal dimension, *Trans. Porous Media*, *4*, 599–612, 1989.

Long, J. C. S., et al., Analog site for fractured rock characterization, annual report FY 1995, *Rep. LBNL-38095*, E. O. Lawrence Berkeley Natl. Lab., Berkeley, Calif., 1995.

Long, P., and B. Wood, Structures, textures, and cooling histories of Columbia River basalt flows, *Geol. Soc. Am. Bull.*, *97*, 1144–1155, 1986.

National Research Council Committee on Fracture Characterization and Fluid Flow, *Rock Fractures and Fluid Flow: Contemporary Understanding and Applications*, Natl. Acad. Press, Washington, D. C., 1996.

Nativ, R., E. Adar, O. Dahan, and M. Geyh, Water recharge and solute transport through the vadose zone of fractured chalk under desert conditions, *Water Resour. Res.*, *31*(2), 253–262, 1995.

Newman, M. E., and F. M. Dunnivant, Results from the large-scale aquifer pumping and infiltration test: Transport of tracers through fractured media, *Rep. INEL-95/146 ER-WAG7-77*, Idaho Natl. Eng. and Environ. Lab., Idaho Falls, 1995.

Nicholl, M. J., R. J. Glass, and H. A. Nguyen, Wetting front instability in an initially wet unsaturated fracture, paper presented at Fourth

International Conference on High Level Radioactive Waste Management, Am. Nucl. Soc., Las Vegas, Nev., 1993.

Nicholl, M. J., R. J. Glass, and S. W. Wheatcraft, Gravity-driven infiltration instability in initially dry nonhorizontal fractures, *Water Resour. Res.*, *30*(9), 2533–2546, 1994.

Or, D., and T. A. Ghezzehei, Dripping into subterranean cavities from unsaturated fractures under evaporative conditions, *Water Resour. Res.*, *36*(2), 381–394, 2000.

Persoff, P., and K. Pruess, Two-phase flow visualization and relative permeability measurement in natural rough-walled rock fractures, *Water Resour. Res.*, *31*(5), 1175–1186, 1995.

Peters, R. R., and E. A. Klavetter, A continuum model for water movement in an unsaturated fractured rock mass, *Water Resour. Res.*, *24*(3), 416–430, 1988.

Peterson, J. E., Jr., S. Hubbard, K. H. Williams, E. L. Majer, and P. Zawislanski, Moisture content estimation using crosshole radar measurement, *Eos Trans. AGU*, *78*(17), Spring Meet. Suppl., S166, 1997.

Priest, S. D., *Discontinuity Analysis for Rock Engineering*, Chapman and Hall, New York, 1993.

Pruess, K., A mechanistic model for water seepage through thick unsaturated zones in fractured rocks of low matrix permeability, *Water Resour. Res.*, *35*(4), 1039–1052, 1999.

Pruess, K., B. Faybishenko, and G. S. Bodvarsson, Alternative concepts and approaches for modeling flow and transport in thick unsaturated zones of fractured rocks, *J. Contam. Hydrol.*, *38*, 281–322, 1999.

Sorenson, K. S., Jr., A. H. Wylie, and T. R. Wood, Test Area North hydrogeologic studies test plan: Operable Unit 1-07B, *Rep. INEL-96/0105*, Idaho Natl. Eng. and Environ. Lab., Idaho Falls, 1996.

Su, G. W., J. T. Geller, K. Pruess, and F. Wen, Experimental studies of water seepage and intermittent flow in unsaturated, rough-walled fractures, *Water Resour. Res.*, *35*(4), 1019–1038, 1999.

Tomkeieff, S. I., The basalt lavas of the Giant's Causeway district of northern Ireland, *Bull. Volcanol.*, *2*(6), 89–146, 1940.

Unger, A. J., G. S. Bodvarsson, B. Faybishenko, and A. M. Simmons, Preferential flow paths in variably fractured basalt at the Box Canyon site, *Rep. LBNL-44613*, E. O. Lawrence Berkeley Natl. Lab., Berkeley, Calif., 1999.

Vandevivere, P., P. Baveye, D. Sanchez de Lozada, and P. DeLeo, Microbial clogging of saturated soils and aquifer materials: Evaluation of mathematical models, *Water Resour. Res.*, *31*(9), 2173–2180, 1995.

Vasco, D. W., J. E. Peterson Jr., and K. H. Lee, Ground-penetrating radar velocity tomography in heterogeneous and anisotropic media, *Geophysics*, *2*(6), 1758–1773, 1997.

Wang, J. S. Y., and T. N. Narasimhan, Unsaturated flow in fractured porous media, in *Flow and Contaminant Transport in Fractured Rock*, edited by J. Bear, C.-F. Tsang, and G. de Marsily, pp. 325–394, Academic, San Diego, Calif., 1993.

Warren, J. E., and P. J. Root, The behavior of naturally fractured reservoirs, *Soc. Pet. Eng. J.*, *228*, 245–255, 1963.

Weisbrod, N., R. Nativ, D. Ronen, and E. Adar, On the variability of fracture surfaces in unsaturated chalk, *Water Resour. Res.*, *34*(8), 1881–1888, 1998.

Welhan, J. A., and M. F. Reed, Geostatistical analysis of regional hydraulic conductivity variations in the Snake River Plain aquifer, eastern Idaho, *Geol. Soc. Am. Bull.*, *109*, 855–868, 1997.

Wood, T. R., and G. T. Norrell, Integrated large-scale aquifer pumping and infiltration tests: Groundwater pathways OU 7-06: Summary report, *Rep. INEL-96/0256*, Idaho Natl. Eng. and Environ. Lab., Idaho Falls, 1996.

Zawislanski, P. T., and B. Faybishenko, New casing and backfill design for neutron access boreholes, *Ground Water J.*, *37*(1), 33–37, 1999.

C. Doughty, B. Faybishenko, and P. T. Zawislanski, Earth Sciences Division, E. O. Lawrence Berkeley National Laboratory, 1 Cyclotron Road, MS 90-1116, University of California, Berkeley, CA 94720. (bfayb@lbl.gov)

J. S. Jacobsen, Lawrence Livermore National Laboratory, L-103, Livermore, CA 94550.

J. C. S. Long, Mackay School Mines, University of Nevada, M/S 168, Reno, NV 89557-0025.

J. Lore, BP Amoco Exploration, 570 Westlake Park Blvd., Fl 6, Houston, TX 77079.

M. Steiger, Erler and Kalinowski, Inc., 1730 S. Amphlett Blvd., Suite 320, San Mateo, CA 94402.

T. R. Wood, Idaho National Engineering and Environmental Laboratory, P.O. Box 1625/MS 3953, Idaho Falls, ID 83415.

(Received March 8, 1999; revised May 5, 2000;
accepted May 10, 2000.)